

Validating and modeling the impact of high-frequency rapid antigen screening on COVID-19 spread and outcomes

Beatrice Nash

E25Bio, Inc.

Anthony Badea

E25Bio, Inc.

Ankita Reddy

E25Bio, Inc.

Miguel Bosch

E25Bio, Inc.

Nol Salcedo

E25Bio, Inc.

Adam Gomez

E25Bio, Inc.

Alice Versiani

Universidade Federal de Minas Gerais

Gislaine Dutra

Faculdade de Medicina de São José do Rio Preto (FAMERP)

Thayza dos Santos

Faculdade de Medicina de São José do Rio Preto (FAMERP)

Bruno Milhim

Faculdade de Medicina de São José do Rio Preto (FAMERP)

Marilia Moraes

Faculdade de Medicina de São José do Rio Preto (FAMERP)

Guilherme Campos

Faculdade de Medicina de São José do Rio Preto (FAMERP)

Flávia Quieroz

Faculdade de Medicina de São José do Rio Preto (FAMERP)

Andreia Francesli Negri Reis

Prefeitura Municipal de Sao Jose do Rio Preto

Mauricio Nogueira

Faculdade de Medicina de São José do Rio Preto <https://orcid.org/0000-0003-1102-2419>

Elena Naumova

Tufts University Friedman School Nutrition Science and Policy <https://orcid.org/0000-0002-9562-4734>

Irene Bosch

E25Bio

Bobby Brooke Herrera (✉ bbherrera@e25bio.com)

E25Bio, Inc.

Article

Keywords: Computational Modeling, Quantitative Real-time Polymerase Chain Reaction, Antigen-based Surveillance, Societal Re-opening

Posted Date: November 16th, 2020

DOI: <https://doi.org/10.21203/rs.3.rs-104765/v1>

License:  This work is licensed under a Creative Commons Attribution 4.0 International License.

[Read Full License](#)

1 **Validating and modeling the impact of high-frequency rapid antigen screening on COVID-**
2 **19 spread and outcomes**

3

4 Authors: Beatrice Nash^{1,2*}, Anthony Badea^{1,3*}, Ankita Reddy^{1,4*}, Miguel Bosch^{1,5}, Nol Salcedo¹,
5 Adam R. Gomez¹, Alice Versiani⁶, Gislaine Celestino Dutra Silva⁶, Thayza Maria Izabel Lopes
6 dos Santos⁶, Bruno H. G. A. Milhim⁶, Marilia M Moraes⁶, Guilherme Rodrigues Fernandes
7 Campos⁶, Flávia Quieroz⁶, Andreia Francesli Negri Reis⁶, Mauricio L. Nogueira⁶, Elena N.
8 Naumova⁷, Irene Bosch^{1,8}, Bobby Brooke Herrera^{1,9†}

9

10 *These authors contributed equally to this work.

11

12 Affiliations:

13 ¹E25Bio, Inc., Cambridge, MA, USA

14 ²Department of Computer Science, Harvard University School of Engineering and Applied
15 Sciences, Cambridge, MA, USA

16 ³Department of Physics, Harvard University, Cambridge, MA, USA

17 ⁴Perelman School of Medicine, University of Pennsylvania, Philadelphia, PA, USA

18 ⁵InfoGeosciences LLC, Houston, TX, USA

19 ⁶Faculdade de Medicina de São José do Rio Preto (FAMERP), São José do Rio Preto, Brazil

20 ⁷Division of the Nutrition Epidemiology and Data Science, Friedman School of Nutrition Science
21 and Policy, Tufts University, Boston, MA, USA

22 ⁸Department of Medicine, Mount Sinai School of Medicine, New York, NY, USA

23 ⁹Department of Immunology and Infectious Diseases, Harvard T.H. Chan School of Public Health,
24 Boston, MA, USA

25

26 †Corresponding Author. BBH, email: bbherrera@e25bio.com

27

28 Short Title: Modeling rapid antigen testing on COVID-19 spread

29

30

31

32

33

34

35

36

37

38

39

40

41

42

43

44

45

46 **Abstract**

47 High frequency screening of populations has been proposed as a strategy in facilitating
48 control of the COVID-19 pandemic. We use computational modeling, coupled with clinical data
49 from rapid antigen tests, to predict the impact of frequent viral antigen rapid testing on COVID-
50 19 spread and outcomes. Using patient nasal or nasopharyngeal swab specimens, we demonstrate
51 that the sensitivity/specificity of two rapid antigen tests compared to quantitative real-time
52 polymerase chain reaction (qRT-PCR) are 80.0%/91.1% and 84.7%/85.7%, respectively;
53 moreover, sensitivity correlates directly with viral load. Based on COVID-19 data from three
54 regions in the United States and São José do Rio Preto, Brazil, we show that high frequency,
55 strategic population-wide rapid testing, even at varied accuracy levels, diminishes COVID-19
56 infections, hospitalizations, and deaths at a fraction of the cost of nucleic acid detection via qRT-
57 PCR. We propose large-scale antigen-based surveillance as a viable strategy to control SARS-
58 CoV-2 spread and to enable societal re-opening.

59

60

61

62

63

64

65

66

67

68

69 INTRODUCTION

70 The COVID-19 pandemic has taken an unprecedented toll on lives, wellbeing, healthcare
71 systems, and global economies. As of 4 November 2020, there have been more than 47.6 million
72 confirmed cases globally with more than 1 million confirmed deaths ¹. However, these numbers
73 and the current mapping of disease spread present an incomplete picture of the outbreak largely
74 due to the lack of adequate testing, particularly as undetected infected cases are the main source
75 of disease spread ²⁻⁷. It is estimated that the reported detection rate of actual COVID-19 cases is
76 only 1-2% ⁵. As of November 2020, the United States, Brazil, and India remain the top three
77 countries with the highest number of COVID-19 cases and deaths worldwide. As countries begin
78 to re-open their economies, a method for accessible and frequent surveillance of COVID-19, with
79 the necessary rapid quarantine measures, is crucial to prevent the multiple resurgences of the
80 disease.

81 The current standard of care rightfully places a strong focus on the diagnostic limit of
82 detection, yet frequently at the expense of both cost and turnaround time. This situation has
83 contributed to limited population testing largely due to a dearth of diagnostic resources.
84 Quantitative real-time polymerase chain reaction (qRT-PCR) is the gold-standard method for
85 clinical diagnosis, with high sensitivity and specificity, but these tests are accompanied by the need
86 for trained personnel, expensive reagents and instrumentation, and a significant amount of time to
87 execute. Facilities offering qRT-PCR sometimes require a week or longer to complete and return
88 the results to the patient. During this waiting period the undiagnosed individual may spread the
89 infection and/or receive delayed medical treatment. Moreover, due to the cost and relative
90 inaccessibility of qRT-PCR in both resource-limited and abundant settings, large-scale screening
91 using qRT-PCR at frequent intervals remains impractical to identify infected but asymptomatic or

92 mildly symptomatic infections. Numerous studies have reported asymptomatic COVID-19 cases
93 as well as a variation in viral load within and between individuals at different time points,
94 suggesting the need for more frequent testing for informative surveillance.

95 Technologies alternate to qRT-PCR, such as rapid viral antigen detection, clustered
96 regularly interspaced short palindromic repeats (CRISPR), and loop-mediated isothermal
97 amplification (LAMP) of SARS-CoV-2 provide potential large-scale screening applications, yet
98 their implementation is stymied by requirements for qRT-PCR-like accuracy before they can reach
99 the market ⁸. In countries such as India, where the qRT-PCR resources would not be sufficient to
100 cover monitoring of the population, the use of rapid antigen tests is well underway^{9,10}. In early
101 May 2020, the United States Food and Drug Administration (FDA) authorized the first antigen
102 test for the laboratory detection of COVID-19, citing a need for testing beyond molecular and
103 serological methods. Antigen testing detects the viral proteins rather than nucleic acids or human
104 antibodies, allowing for detection of an active infection with relative ease of sample collection and
105 assay. These rapid assays – like other commercially-available rapid antigen tests - can be mass-
106 produced at low prices and be administered by the average person without a laboratory or
107 instrumentation. These tests also take as little as 15 minutes to determine the result, enabling real-
108 time surveillance and/or diagnosis. Although antigen tests usually perform with high specificities
109 (true negative rate), their sensitivity (true positive rate) is often lower when compared to molecular
110 assays. While qRT-PCR can reach a limit of detection as low as 10^2 genome copies per mL, rapid
111 antigen testing detects viral protein that is assumed to correlate with approximately 10^5 genome
112 copies per mL ¹¹.

113 We hypothesize that frequent antigen-based rapid testing even with lower sensitivities
114 compared to qRT-PCR - along with appropriate quarantine measures - can be more effective at

115 decreasing COVID-19 spread than less frequent molecular testing of symptomatic individuals.
116 Keeping in mind the realities of daily testing in resource-limited regions, we also hypothesize that
117 testing frequency can be adjusted according to the prevalence of the disease; that is, an uptick in
118 reported cases should be accompanied by more frequent testing. During the viral incubation period,
119 high infectivity correlates with a high viral load that can be detected by either qRT-PCR or rapid
120 antigen testing¹²⁻¹⁶. Rapid tests thus optimize diagnosis for the most infectious individuals. Studies
121 also point to the relatively small window of time during an individual's incubation period in which
122 the qRT-PCR assay is more sensitive than rapid tests¹².

123 In this study we report the clinical validation of two direct antigen rapid tests for detection
124 of SARS-CoV-2 spike glycoprotein (S) or nucleocapsid protein (N) using retrospectively collected
125 nasopharyngeal or nasal swab specimens. Using the clinical performance data, we develop a
126 modeling system to evaluate the impact of frequent rapid testing on COVID-19 spread and
127 outcomes using a variation of a SIR model, which has been previously used to model COVID-19
128 transmission¹⁷⁻²³. We build on this model to incorporate quarantine states and testing protocols to
129 examine the effects of different testing regimes. This model distinguishes between undetected and
130 detected infections and separates severe cases, specifically, those requiring hospitalization, from
131 those less so, which is important for disease response systems such as intensive care unit triaging.
132 We simulate COVID-19 spread with rapid testing and model disease outcomes in three regions in
133 the United States and São José do Rio Preto, Brazil - the site of the clinical validation study - using
134 publicly available data. To date, COVID-19 modeling describes the course of disease spread in
135 response to social distancing and quarantine measures, and a previous simulation study has shown
136 that frequent testing with accuracies less than qRT-PCR, coupled with quarantine process and
137 social distancing, are predicted to significantly decrease infections^{12,17,23-27}. This is the first

138 modeling system using publicly-available data to simulate how potential public health strategies
139 based on testing performance, frequency, and geography impact the course of COVID-19 spread
140 and outcomes. Our findings suggest that a rapid test, even with sensitivities lower than molecular
141 tests, when strategically administered 2-3 times per week, will reduce COVID-19 spread,
142 hospitalizations, and deaths at a fraction of the cost of nucleic acid testing via qRT-PCR. Modern
143 surveillance systems should be well equipped with rapid testing tools to ensure that disease
144 tracking and control protocols are effective and well-tailored to national, regional, and community
145 needs.

146

147 **RESULTS**

148 **Accuracy of Direct Antigen Rapid Tests Correlate with Viral Load Levels**

149 Rapid antigen tests have recently been considered a viable source for first-line screening,
150 although concerns regarding the accuracy of these tests persist. We clinically validated two
151 different direct antigen rapid tests for the detection of either N or S from SARS-CoV-2 in
152 retrospectively collected nasal or nasopharyngeal swab specimens. Of the total number of nasal
153 swab specimens evaluated by qRT-PCR for amplification of SARS-CoV-2 N, S, and ORF1ab
154 genes, 100 tested positive and 90 tested negative (Table 1-2). The overall sensitivity and specificity
155 of the rapid antigen test for detection of SARS-CoV-2 N, evaluated across the nasal swab
156 specimens, was 80.0% and 91.1%, respectively. Of the total number of nasopharyngeal swab
157 specimens evaluated by qRT-PCR for amplification of SARS-CoV-2 N, RNA-dependent RNA
158 polymerase (RdRp), and envelope (E) genes, 72 tested positive and 49 tested negative (Table 1,
159 Table 3). The overall sensitivity and specificity of the rapid antigen test for detection of SARS-
160 CoV-2 S, evaluated across the nasopharyngeal swab specimens was 84.7% and 85.7%,

161 respectively. Altogether, our data demonstrate that the sensitivity of the rapid antigen tests are
162 positively correlated to the viral load level (Table 1, Figure S1).

163 The Ct value indirectly quantifies the viral RNA copy number related to the viral load of
164 the sample for the specific assay^{28,29}. Ct values represent the number of qRT-PCR cycles at which
165 generated fluorescence crosses a threshold during the linear amplification phase; Ct values are
166 therefore inversely related to the viral load. The sensitivity of both rapid antigen tests increases as
167 Ct value decreases (Table 1). Moreover, because the Ct value is a variable unit based upon qPCR
168 protocol and instrumentation, we evaluated sensitivity against the percentile of positive cases
169 conditioned to Ct and found similar results. The sensitivity of the rapid antigen test for detection
170 of SARS-CoV-2 N increased from 80.0% at Ct values <40 to 95.8% at Ct values <20
171 (Supplementary Fig. 1a). Similarly, the sensitivity of the rapid antigen test for detection of SARS-
172 CoV-2 S increased from 84.7% at Ct values <35 to 100.0% at Ct values <15 (Supplementary Fig.
173 1b). Taken together, the clinical data shows that the rapid antigen test performs with increasing
174 accuracy for individuals with a higher viral load, and potentially the most infectious¹³⁻¹⁶.

175

176 **An Enhanced Epidemiological SIDHRE-Q Model**

177 We propose an enhanced epidemiological modeling system, *SIDHRE-Q*, a variant of the
178 classical SIR model in order to expand our clinical validation study and to understand the effects
179 of using frequent rapid tests such as the rapid antigen test on COVID-19 outbreak dynamics. The
180 changes we make to the basic model to encompass the unique characteristics of the COVID-19
181 pandemic are similar to those presented by Giordano et al. (16) (Fig. 1, Supplementary Fig. 2).
182 The differential equations governing the evolution of the *SIDHRE-Q* model and descriptions of
183 the parameter values are provided in the methods section (Equation 2, Table 4).

184 An individual that begins in **S** may either transition to a Quarantine Uninfected (**Q-U**) state
185 via a false positive result or to an Infected Undetected (**I**) state via interaction with an infected
186 individual. Should an individual in **S** move into **Q-U**, they are quarantined for 14 days before
187 returning to **S**, a time period chosen based on current knowledge of the infectious period of the
188 disease. One could also conceive of an effective strategy in which individuals exit quarantine after
189 producing a certain number of negative rapid tests in the days following their initial positive result
190 or confirm their negative result using qRT-PCR.

191 Given that those diagnosed are predominantly quarantined, individuals in **I** interact more
192 with the **S** population than do those in Infected Detected (**D**). Therefore, the infectious rate for **I** is
193 assumed to be significantly larger than for **D**. Furthermore, a region's ability to control an outbreak
194 is directly related to how quickly and effectively people in **I** test into **D**, reducing their
195 infectiousness through quarantine. This study, in particular, highlights the critical role frequency
196 of testing, along with strict quarantine, has in mitigating the spread of the disease and provides
197 specific testing strategies based on rapid tests we predict to be highly effective.

198 In this model, we assume that individuals receive a positive diagnosis before developing
199 severe symptoms and that those with symptoms severe enough to be potentially fatal will go to the
200 hospital. If an individual develops symptoms, we assume they are tested daily until receiving a
201 positive result; hence, before severe symptoms develop, they will be diagnosed with high
202 probability. Those who do not develop symptoms are tested according to the frequency of tests
203 administered to the general population. Therefore, there is no modeled connection between **I** and
204 **H** or between **I** and **E**. Removing these assumptions would have negligible impact on the results
205 as these flows are very small.

206 Should an individual test positive and transition to **D**, they may either develop serious
207 symptoms requiring care or recover. Those who develop serious symptoms and transition to state
208 **H** will then transition to either **R** or **E**. The recovered population is inevitably tested, as infected
209 individuals may recover without being detected. Therefore, the Quarantined Recovered (**Q-R**)
210 state is introduced with the same connections to **R** as the connections between **S** and **Q-U**. Though
211 the reinfection rate of SARS-CoV-2 has been a point of recent debate, it is assumed that the number
212 of re-infected individuals is small³⁰⁻³⁴. Therefore, individuals cannot transition from **R** to **S**, hence
213 the separately categorized quarantined populations.

214 We considered several variations and extensions of the *SIDHRE-Q* model. In simulations,
215 we tested additional states, such as those in the *SIDARTHE* model, which include distinctions
216 between symptomatic and asymptomatic cases for both detected and undetected populations¹⁷.
217 Incorporating information about the correlations between viral load and infectivity and sensitivity
218 were also considered. Altogether, our modeling system has been well tuned to predict the impact
219 of high frequency rapid testing on COVID-19 spread and outcomes.

220

221 **Frequent Rapid Testing with Actionable Quarantining Dramatically Reduces Disease** 222 **Spread**

223 In order to demonstrate how strategies could affect the disease spread in different
224 geographies and demographics, we used surveillance data obtained from regions of varying
225 characteristics: the state of Massachusetts (MA), New York City (NYC), Los Angeles (LA), and
226 São José do Rio Preto (SJRP), Brazil, the site of the rapid antigen test clinical validation study.
227 These regions are also selected in our study due to the readily available surveillance data provided
228 by the local governments. We fit the model to the data from each region starting 1 April 2020. At

229 this time point the disease reportedly is most advanced in NYC and least advanced in SJRP, Brazil
230 with estimated cumulative infection rates of 7.11% and 0.12%, respectively.

231 After calibrating the *SIDHRE-Q* model, the disease spread is observed with varying
232 validated rapid antigen test performances and frequencies (Fig. 2). Sensitivity (the ratio of true
233 positives to the total number of positives) and specificity (the ratio of true negatives to the total
234 number of negatives) compared to gold-standard qRT-PCR were used as measures of test
235 accuracy.

236 The rapid test frequency is varied while maintaining an accuracy of 80% sensitivity and
237 90% specificity, comparable to our clinical data collected in SJRP, Brazil. These testing scenarios
238 are then compared to symptomatic testing, in which individuals receive a rapid test only when
239 presenting symptoms, via either a rapid test or qRT-PCR. Since the primary testing regiment
240 deployed in MA, LA, NYC and SJRP, Brazil is qRT-PCR-based and focused on symptomatic
241 individuals, the symptomatic testing protocol via qRT-PCR is directly estimated from the data to
242 be the rate ν (Table 4).

243 The difference between the qRT-PCR and rapid test simulations (red and orange lines,
244 respectively) is therefore only sensitivity of testing (Fig. 2). We assumed that test outcome
245 probability is a function only of whether an individual is infected and independent of other factors;
246 one can consider this a lower bound on effectiveness of a strategy, as sensitivity and infectivity
247 are often positively correlated with antigen testing.

248 To better understand the effect of rapid testing frequency and performance on healthcare
249 capacity and mortality rates, we simulate the testing strategy with 30%-90% sensitivity each with
250 80% or 90% specificity against the symptomatic testing strategy (Supplementary Fig. 3).

251 As per our hypothesis, frequency and symptom-based testing dramatically reduced
252 infections, simultaneous hospitalizations, and total deaths when compared to the purely symptom-
253 based testing regiments, and infections, hospitalization, and death were reduced as frequency
254 increased. Although testing every day was clearly most effective, even testing every fourteen days
255 with an imperfect test gave an improvement over symptomatic testing with qRT-PCR. While the
256 strategy works best when implemented at the very beginning of an outbreak, as demonstrated by
257 the results in SJRP, Brazil, it also works to curb an outbreak that is already large, as demonstrated
258 by the results in NYC. The difference between frequencies is more noticeable when the testing
259 strategy is applied to the outbreak in NYC, leading us to hypothesize that smaller outbreaks require
260 a lower testing frequency than larger ones; note the difference between the dependence on
261 frequency to curb a small initial outbreak in SJRP, Brazil versus a large one in NYC (Fig. 3).

262 For test performance of 80% sensitivity and 90% specificity, the percent of the population
263 that has been infected in total from the beginning of the outbreak to mid-July drops from 18%
264 (MA), 11% (LA), 26% (NYC), and 11% (SJRP, Brazil) to 3%, 2%, 12%, and 0.26%, respectively,
265 using a weekly rapid testing and quarantine strategy (with regards to predictions of overall
266 infection rates, other studies based on seroprevalence and epidemiological predictions have
267 reached similar conclusions ^{35,36}). If testing is increased to once every three days, these numbers
268 drop further to 1.6% (MA), 1.4% (LA), 9.5% (NYC), and 0.19% (SJRP, Brazil) (Table S1).

269 To further examine the relationship between frequency and sensitivity, we modeled the
270 maximum number of individuals in a given state over the 105-day time period for four geographic
271 regions (Fig. 3, Supplementary Fig. 4). In all four geographic regions, as frequency of testing
272 increases, the total infections, maximum simultaneous hospitalizations, and total deaths converge
273 to small percentages regardless of the sensitivity at high frequencies. It is clear that the difference

274 in frequency required to achieve the same result using tests of differing sensitivities is very small.
275 For example, we predict that for the outbreak in LA, a testing strategy started on 1 April of every
276 10 days using a test of sensitivity 90% would have resulted in 2.5% of the population having been
277 infected, while using a test of sensitivity 30% would require a strategy of every 5 days to achieve
278 the same number. Thus, we conclude that frequency is more important than sensitivity in curbing
279 the spread, and a large range of sensitivities prove effective when testing sufficiently often
280 (Supplementary Fig. 4). How frequently, exactly, depends on the specific outbreak and what stage
281 it is in, which leads us to the location-based deployment strategy discussed in a later section.
282 Frequency of testing can be significantly reduced to effectively contain the disease once the initial
283 outbreak has been controlled; it is clear that this takes only a matter of weeks (Fig. 2).

284 On the other hand, according to the specificity of the rapid test and the quarantine duration,
285 larger testing frequency result in a larger percent of the population quarantined (Fig. 2). Assuming
286 a 90% rapid test specificity and 14-day quarantine duration, for the 1-, 3- and 7-day frequencies
287 almost 60%, 38% and 20% of the population, respectively, would be quarantined. This figure may
288 be reduced with additional rules for exiting quarantine early, such as after complementary testing.
289 An example of such a strategy is that individuals who test positive are required to either quarantine
290 for two weeks or produce two consecutive negative rapid tests in the two days following their
291 positive result. Assuming 80% sensitivity and 90% specificity, those individuals will reenter the
292 public while still infected with probability 0.04. If uninfected, that individual will exit quarantine
293 after two days with probability 0.81. However, a compromise between the reduction of infections
294 and the proportion of the population in quarantine would be part of the planning for the appropriate
295 testing protocol in each community or region.

296 Additionally, while high frequency may be necessary to contain a large outbreak initially,
297 relatively infrequent testing, such as every one or two weeks, is sufficient to keep controlled
298 outbreaks small, while reducing the number of quarantined individuals to less than 10% of the
299 population using a two-week mandatory quarantine.

300
301 **A County-Based Testing Strategy Offers a Cost-effective Approach to Large-scale COVID-**
302 **19 Surveillance**

303 To examine the effects of resource-strategic testing schemes, we modeled the COVID-19
304 prevalence by varying testing frequency across counties of California. For this analysis, only
305 California was analyzed because of the accessibility of the county level data and the variability of
306 spread dynamics of the outbreaks between counties. In this scheme, the percent of active infected
307 detected individuals in a county determines the frequency of testing. We define thresholds for the
308 number of active detected infections that, when hit, initiate testing protocols of different
309 frequencies depending on the threshold hit. We first tested evenly spaced thresholds for the number
310 of detected active infections up to 1% of the population, but later adopted thresholds that were
311 determined according to Equation 1. In Equation 1, D = population of state \mathbf{D} at the time of testing.
312 T = number of active infections which, if reached, initiates everyday testing. The days between
313 tests are rounded to the closest integer value.

$$\text{Days between tests} = \max(1, 2\log_2(T/D) + 1)$$

314
315 (1)

316 The days between tests are chosen such that the detected active infections should remain near to
317 or below T . If the initial detected active infections are greater than T , then the testing frequency
318 of 1 will cause infections to rapidly drop. Both the threshold at which everyday testing begins and

319 the coefficient of $\log_2 T/D$ can be modified to produce a strategy that is more or less frequent in
320 testing or resource effective; a range of days between tests from 14 days to 1 day are used (Fig.
321 4a). The purpose of this strategy is to tailor testing based on the specific characteristics of local
322 outbreaks in order to mitigate the overall spread faster and more efficiently. A scan over different
323 choices of T is shown in Fig. 4b; the threshold we choose in Fig. 4a is 0.05% because it is successful
324 in curbing the outbreak within the time period we consider. While the choices work for the
325 epidemic in California at the point we start our simulations, 10 April, they do not necessarily reflect
326 the most resource effective choices everywhere. Our analysis could be redone to select the best
327 fine-grained strategy in other states or metropolitan areas.

328 Using a rapid test with a sensitivity of 80% and specificity of 90%, the county-based testing
329 with threshold 0.05% reduces the active infections from 0.94% to 0.0005%, while the uniform
330 strategy with tests administered every 7 days results in double the number of active infections (Fig.
331 4a). As the threshold is reduced, the total cost increases while the cumulative infections, maximum
332 percentage hospitalized, and cumulative deaths all decrease (Fig. 4b). Appropriate choice of
333 threshold is dependent on the severity of outbreaks in a specific region and available resources,
334 both logistically and fiscally. With regional data, such as that from California used to produce Fig.
335 4b, this study can be reproduced to calculate an efficient testing strategy that will effectively curb
336 outbreaks of differing severities in any geographic entity.

337 Strategy B in Fig. 4 consists of qRT-PCR testing uniformly applied to the highlighted
338 population with a frequency of once weekly. The average cost per person per day is just under \$15.
339 Despite this frequency and the accuracy of qRT-PCR, the strategy does not succeed in curbing the
340 spread as fast as strategy A, which uses a testing sensitivity and specificity of 80% and 90%,
341 respectively, and testing frequency that vary between counties depending on the proportion of their

342 population that is currently infected. The total cost for strategy A is estimated at a fraction of the
343 other at \$1.53 per person per day.

344

345 **DISCUSSION**

346 In this study we examine the potential effects of a novel testing strategy to limit the spread
347 of SARS-CoV-2 utilizing rapid antigen test screening approaches. Our clinical data and *SIDHRE-*
348 *Q* modeling system demonstrate that 1) frequent rapid testing even at a range of accuracies is
349 effective at reducing COVID-19 spread, 2) rapid antigen tests are a viable source for this strategy
350 and diagnose the most infectious individuals, and 3) strategic geographic-based testing can
351 optimize disease control with the amount of available resources. The public has witnessed and
352 experienced symptomatic individuals being denied testing due to shortages, and few testing
353 structures for asymptomatic or mildly symptomatic individuals – a significant source of disease
354 spread. Though several factors contributed to the stymied early response measures, such as
355 lockdown and quarantine protocols and adherence, severe testing bottlenecks are a significant
356 culprit ³⁷⁻³⁹. Early control measures have been shown to decrease lives lost by several orders of
357 magnitude ⁴⁰. These challenges, though exacerbated during the early months of the pandemic,
358 remain at the forefront of the public health crises.

359 Diagnosis of SARS-CoV-2 infection by qRT-PCR is the current standard of care, yet
360 remains expensive and requires a laboratory and experienced personnel for sample preparations
361 and experimentation. The turnaround time for results can be up to 10 days, preventing people from
362 either leaving quarantine if they are negative, or delaying critical care and infecting others if they
363 are positive ⁴¹. This current testing scheme moreover yields incomplete surveillance data on which
364 response efforts such as societal reopening and hospital management depend. Though qRT-PCR

365 is considered the gold-standard diagnostic method because of its high sensitivity and specificity,
366 the logistical hurdles render it unrealistic for large-scale screening.

367 As qRT-PCR remains impractical for this strategy, and rapid tests are facing regulatory
368 challenges because they do not perform with qRT-PCR-like accuracy, rapid test screening is either
369 nonexistent in several countries or symptom-based. Even under best-case assumptions, findings
370 have shown that symptom and risk-based screening strategies miss more than half of the infected
371 individuals⁴². Some have argued that the need for widespread testing is overstated due to the
372 variability in test sensitivity and specificity⁴³. Here, we present alternative large-scale diagnostic
373 tools to qRT-PCR, and show that test performance, though valuable, is secondary to widespread
374 test frequency, which is enabled by accessibility and turnaround time. Furthermore, test
375 affordability is essential for the successful implementation in communities most affected by
376 infection and will to speed up the safe opening and functioning of the viral sectors of the economy.

377 Giordano et al. has modeled the evolution of SARS-CoV-2 spread, introducing a diagnosed
378 state to elucidate the importance of population-wide testing¹⁷. Mina et al. has examined how
379 various test sensitivities and frequencies affect the reproductive number¹². We build upon these
380 findings to show how in affected United States and Brazil regions, population-wide frequent and
381 rapid testing schemes, with sensitivities ranging from 30%-90%, can be more effective in curbing
382 the pandemic than a PCR-based scheme. Integrating real-world surveillance and clinical data into
383 our modeling system has allowed us to incorporate regional differences - such as variances in
384 healthcare access, state health policy and adherence, state GDP, and environmental factors - under
385 the same model. Significantly, our findings hold true across Massachusetts, New York City, Los
386 Angeles, and São José do Rio Preto, Brazil. We also present the economic considerations of these
387 testing regimes, showing that widespread rapid testing is more cost efficient than less frequent

388 qRT-PCR testing. In line with these economic considerations, our model demonstrates the
389 effectiveness of a geographic-based frequent testing regime, in which high disease prevalence
390 areas receive more frequent testing than low disease prevalence areas.

391 Since COVID-19 is known to affect certain demographics differently, modeling would
392 benefit from incorporating demographic information correlated with disease progression and
393 spread to define sub-models and sets of parameters accordingly. Age, pre-existing conditions, job
394 types, and density of population are examples of possible categories, each of which influence the
395 risk of contracting and/or dying from COVID-19. Further studies would benefit from incorporating
396 these ideas to better understand the effectiveness of rapid testing on identifying potential super
397 spreading events. Future public health prevention programs should use the proposed modeling
398 system to develop and test scenarios for precision testing and prevention.

399 Our findings also point to low-cost tools for implementation of this testing strategy, such
400 as a rapid antigen-based test for the detection of SARS-CoV-2 proteins. We show that the rapid
401 antigen tests perform with a range of accuracies under which disease spread can be dramatically
402 mitigated under our model. Notably, the sensitivity is correlated to the individual's viral load,
403 effectively diagnosing those who are potentially the most infectious with the highest accuracy. Our
404 findings are significant because rapid antigen tests are cheaper than qRT-PCR, can be mass
405 produced to millions per day, present results within 15 minutes, and can be administered by a
406 nonexpert without a lab or special equipment.

407 There are several policy implications for these findings. First, our model supports that
408 systems of high frequency rapid testing should be implemented as a first-line screening method.
409 This can be first enabled by a more holistic regulatory evaluation of rapid diagnostics, such that
410 policy emphasizes accessibility and turnaround time even under a range of accuracies. One can

411 imagine a less accurate, though rapid method of first-line screening in schools, public
412 transportation, and airports, or even at home, and a qRT-PCR-based method for second-line
413 screening (testing those who present severe symptoms or have been in contact with infected
414 individuals, testing in a clinical setting, etc). Second, our cost analysis and rapid antigen test data
415 present a viable and potentially more cost-effective method for screening. Third, our county-based
416 testing scheme presents a possible method for wide-scale screening while optimizing resources.
417 Future studies should investigate how this selective testing strategy can be applied to different
418 location scales to further inform health policy. Moreover, though our models analyze regions in
419 the United States and Brazil, similar testing strategies can be considered globally in both resource
420 limited and abundant settings due to the higher accessibility of rapid tests compared to qRT-PCR.

421 We emphasize that integral to the effectiveness of diagnostic schemes is 1) the proper
422 adherence to quarantine measures and 2) the combined use of a variety of diagnostic methods
423 including nucleic acid, antigen, and antibody tests. According to these models, rapid antigen tests
424 are an ideal tool for first-line screening. Clinical molecular tests such as qRT-PCR are vital to the
425 diagnostic landscape, particularly to re-test suspected cases that were negative on the rapid test.
426 Because rapid tests present a higher rate of false negatives, methods such as qRT-PCR remain
427 integral to second-line screening. Antibody tests provide important information for immunity and
428 vaccination purposes as well as epidemiological surveillance. This model also assumes that
429 individuals will quarantine themselves before being tested and for 14 days following a positive
430 diagnostic result.

431 Our simulations combined with real-world data demonstrate a robust modeling system and
432 elucidates the significance of this novel testing strategy. However, there are important limitations
433 to be considered. Differences in disease reporting between the geographical regions and the

434 incomplete nature of COVID-19 surveillance data, often due to the lack of testing, are not
435 considered in the model. It is imperative that the testing results, hospitalization and death statistics,
436 and changes in protocol are reported in real-time to scientists and policy makers so that models
437 can be accurately tuned as the pandemic develops. The model also does not take into account
438 infrastructural limitations such as hospital capacity. Though the rapid antigen test offers several
439 advantages such as affordability, fast turnaround time, and ease of mass production, we are also
440 assuming that there are systems in place to implement frequent and safe low-cost screening across
441 different communities and settings.

442 Our model underscores the need for a point-of-care or at-home test for frequent screening,
443 particularly as lockdown restrictions ease. Regulatory agencies can work towards evaluating rapid
444 tests to alternative standards other than comparison to high sensitivity molecular diagnostics, as
445 our model shows that frequency and scale of testing may overcome lower sensitivities. Rather, we
446 could refocus policy to implement first-line screening that optimizes accuracy with efficiency and
447 equitability.

448

449

450

451

452 **METHODS**

453 **Development of Direct Antigen Rapid Tests for the Detection of SARS-CoV-2**

454 We developed a direct antigen rapid test for the detection of the nucleocapsid protein or
455 spike glycoprotein from SARS-CoV-2 in nasal or nasopharyngeal swab specimens as previously
456 described ⁴⁴. Briefly, the rapid antigen tests are immunochromatographic format with a visual

457 readout using anti-N or anti-S mouse monoclonal antibodies (E25Bio, Inc., Cambridge, MA, USA)
458 that are either coupled to 40 nm gold nanoparticles (Abcam, Cambridge, UK) or adsorbed to
459 nitrocellulose membranes (Sartorius, Goettingen, Germany). Each rapid antigen test has a control
460 area adjacent to the paper absorbent pad; the control is an anti-mouse Fc domain antibody (Leinco
461 Technologies, Fenton, MO, USA) that will capture any of the antibody-conjugated gold
462 nanoparticles to generate a control visual signal. A visual signal at the test area reflects SARS-
463 CoV-2 N or S that is “sandwiched” between an anti-N or anti-S antibody adsorbed to the
464 nitrocellulose membrane and a second anti-N or anti-S antibody covalently coupled to visible gold
465 nanoparticles.

466

467 **Validation of Direct Antigen Rapid Test for the Detection of SARS-CoV-2**

468 In a retrospective study of nasal swab specimens from human patients, we compared the
469 accuracy of the rapid antigen test for detection of SARS-CoV-2 N to the viral loads of individuals.
470 Nasal swab specimens (n=190) were tested following approved human subjects use protocols. The
471 nasal swab specimens were banked frozen from suspected patients submitted to PATH for routine
472 COVID diagnosis. Prior to using the rapid test, the nasal swab specimens were validated by qRT-
473 PCR using the FDA EUA ThermoFisher/AppliedBiosystems TaqPATH COVID-19 Combo Kit
474 (ThermoFisher, Waltham, MA USA). The primary study under which the samples and data were
475 collected received ethical clearance from the PATH Research Ethics Committee, protocol number
476 00004244. The nasal swab specimens were de-identified, containing no demographic data, prior
477 to analysis.

478 The nasal swabs were originally collected in 1 mL PBS, where 50 μ l was mixed with 50 μ l
479 of Solution Buffer (0.9% NaCl and 0.1% Triton X-100). The 100 μ l mixture was then pipetted

480 onto the rapid antigen test for SARS-CoV-2 nucleocapsid detection and allowed to react for 15
481 minutes. After processing of the rapid antigen test, the visual positive or negative signal was
482 documented.

483 Additionally, in a retrospective study of nasopharyngeal swab specimens from human
484 patients, we compared the accuracy of the rapid antigen test to the viral load of individuals.
485 Nasopharyngeal swab specimens (n = 121) were tested in Brazil following approved human
486 subjects use protocols. The age of study participants ranged from 1 to 95 years with an overall
487 median of 37 years (interquartile range, 27–51 years), and 62% were female. The demographic
488 summary of the patients are included in Table S2. The nasopharyngeal swab specimens were
489 banked refrigerated or frozen samples from suspected patients submitted to the lab for routine
490 COVID diagnosis. Prior to using the rapid test, the nasopharyngeal swab samples were validated
491 by qRT-PCR using GeneFinderTM COVID-19 Plus RealAmp Kit (OSANGHealthcare, Anyang-si,
492 Gyeonggi-do, Republic of Korea I). The primary study under which the samples and data were
493 collected received ethical clearance from the Faculdade de Medicina de São José do Rio Preto
494 (FAMERP), protocol number 31588920.0.0000.5415. All excess samples and corresponding data
495 were banked and de-identified prior to the analyses.

496 Nasopharyngeal swab specimens (1 mL) were concentrated using Vivaspin 500 centrifugal
497 concentrator (Sartorius, Goettingen, Germany) at 12,000 x g for 10 minutes. The concentrated
498 nasopharyngeal swab specimen retentate was transferred to a collection tube and the rapid antigen
499 test for SARS-CoV-2 spike detection was inserted into the tube with the retentate and allowed to
500 react for 15 minutes. After processing of the rapid antigen test, the visual positive or negative
501 signal was documented.

502

503 **Data for Modeling**

504 As of August 2020, the United States and Brazil have the highest number of confirmed
505 COVID-19 cases and deaths worldwide, with both countries reporting their first case on 26
506 February 2020)¹. Although several affected US regions could have been modeled, we look at data
507 from Massachusetts, New York, and Los Angeles: these regions each contained “hotspots”, or
508 areas of surging COVID-19 cases, at different points in time during the pandemic and have
509 publicly available government-provided surveillance data. Our model is fit using data over 105
510 days beginning on April 1 for Fig. 2 and Fig. 3, and 105 days beginning on April 10 for Fig. 4 (see
511 “Modeling Parameters” in Methods). In order to understand the various testing proposals on a
512 global scale, we performed our clinical study in and expanded the modeling study to Brazil. The
513 specific data we use to fit our model are cumulative confirmed cases, total deaths, and number of
514 daily hospitalizations due to COVID-19. This surveillance data was retrieved from government-
515 provided online databases^{45–51}.

516

517 **Modeling Parameters**

518 Equation 2 below provides the exact differential equations governing the model.

$$\begin{aligned} dS &= -S(\alpha I + \eta D + \gamma) && + \psi Q_U \\ dI &= -I(\varepsilon + \lambda + \nu) && + S(\alpha I + \eta D) \\ dD &= -D\left(\frac{D+I}{D}\mu + \rho\right) && + I(\nu + \varepsilon) \\ dH &= -H(\sigma + \tau) && + \mu(D + I) \\ dE &= && + \tau H \\ dR &= -\gamma R && + \rho D + \lambda I + \sigma H + \psi Q_R \\ dQ_U &= -\psi Q_U && + \gamma S \\ dQ_R &= -\psi Q_R && + \gamma R \end{aligned} \tag{2}$$

519

520 In order to determine the values of the parameters defining the flows between states, we use a least
521 squares regression performed at seven day intervals in the datasets to which we fit. This allows
522 the model to take into account the time dependent nature of the parameters, which rely on factors
523 such as social distancing regulations and changes in testing capacity. We also fit window sizes
524 between 1 and 21 days and find that while the fit degrades with larger window size, the overall
525 shape of the fits do not change. We choose seven days assuming policy changes take a week to
526 become effective and that reasonable parameters can be expected to change within this time period.
527 Also, the seven day window size accounts for the fact that often data is not reported as diligently
528 over the weekend. Time series of the values of the parameters for the geographic locations
529 discussed in this paper are included in Supplementary Fig. 5.

530 Given the restrictions on data available for the populations of various states, varying all of
531 the parameters results in an over parameterized system. Therefore, a subset of the model
532 parameters are fit while the others are either extracted from other sources; see Table 4. The fitting
533 procedure minimizes the sum of the squared residuals of the total cases, current daily
534 hospitalizations, cumulative deaths, and percentage of total infected individuals currently
535 hospitalized. The first three are present in the data sets while the latter is derived from the estimates
536 of the ratio between infected undetected to infected detected individuals from the CDC Laboratory
537 Seroprevalence Survey Data ⁵². While this ratio changes over time, the percentage of infected
538 individuals developing severe symptoms should remain roughly constant throughout the course of
539 the epidemic in the different locations studied.

540 We consider the data sets for outbreaks in MA, NYC, LA, and SJRP, Brazil ⁴⁵⁻⁵⁰. While
541 each location has testing and fatality information dating back to January, hospitalization data was
542 not included until late March (for NYC and SJRP) and April (for MA and LA). Hence we begin

543 our fitting procedure and testing strategy on 1 April for each of the data sets; by this point, the
544 outbreak is advanced in NYC, substantial in MA, non-negligible, but far from its peak, in LA, and
545 in early stages in SJRP, Brazil. Starting simulations at various stages of the outbreak allows one
546 to see the difference in results between when a testing strategy is administered.

547 In order to determine the effectiveness of the county-based strategy when applied to the
548 state of California, we also fit all of the counties in California with a population greater than 1.5%
549 of that of the entire state and with greater than zero deaths. The results do not depend on these
550 selections, but instead suggest a practical criteria to administer limited resources. The fitting is
551 done starting 10 April for these counties, as at this point the outbreak is sufficiently well-
552 documented in each to successfully model. For the county-level data we compute a seven day
553 running average of each of the data sets to which we then fit in order to smooth out fluctuations in
554 the data, likely due to reporting, which are more significant here than in the other data sets
555 considered, as the county populations are smaller and hence discrepancies impact the smoothness
556 of the data more. The fits for each of the counties can be found in Supplementary Fig. 6.

557 As one can see from Fig. 1, these data sets are particularly not smooth, which indicates
558 inefficiencies in reporting. Additionally, it is difficult to gauge their consistency within the dates
559 provided or to compare between locations, as reporting mechanisms changed over time within the
560 same locations. Despite this lack of consistency, our model and fitting mechanism was successful
561 in reproducing the progress of the outbreak in each data set studied.

562

563 **DATA AVAILABILITY**

564 The authors confirm that the data supporting the findings of this study are available within the
565 article and/or its supplementary materials; any other data will be made available upon request.

566

567 **CODE AVAILABILITY**

568 Full code can be found on github: https://github.com/badeaa3/COVID19_Rapid_Testing. The
569 code is written using python with the packages scipy, numpy, lmfit, matplotlib and plotly⁵³⁻⁵⁷.

570

571 **SUPPLEMENTARY MATERIALS**

572

573 **Supplementary Table 1. Summary of results of COVID-19 outcomes in 3 US Regions and**
574 **Brazil as a result of Frequent Rapid Testing Protocol using SIDHRE-Q Model.**

575

576 **Supplementary Table 2. Demographic and clinical summary of patients evaluated by the**
577 **SARS-CoV-2 Direct Antigen Rapid Test (DART).**

578

579 **Supplementary Fig. 1. Performance of direct antigen rapid test (DART) for the detection of**
580 **SARS-CoV-2 (A) nucleocapsid protein and (B) spike glycoprotein.** Shown are the percentile
581 positive cases of the total positive population conditioned to qRT-PCR Cycle Threshold (Ct).
582 Percentile Positive ranks the samples in order of high Ct to low Ct. DART sensitivity is
583 determined by calculating true positive agreement to qRT-PCR; the plot uses an ax^{b+c} fit and
584 95% confidence intervals for the sensitivity.

585

586 **Supplementary Fig. 2. Graphical scheme displaying the relationships between the stages of**
587 **quarantine and infection in *SIDHRE-Q* model: Q-U, quarantine uninfected; S, susceptible**
588 **(uninfected); I, infected undetected (pre-testing and infected); D, infected detected (infection**

589 diagnosis through testing); **H**, hospitalized (infected with life threatening symptom progression);
590 **R**, recovered (healed); **E**, extinct (dead); and **Q-R**, quarantine recovered (healed but in
591 quarantine by false positive testing).

592

593 **Supplementary Fig. 3. COVID-19 Outcomes as a result of Frequent Rapid Testing Protocol**
594 **with variable test performances using *SIDHRE-Q* Model.** The Cumulative Detected Infected,
595 Hospitalized, Deceased, Active Infections, Recovered, and Quarantined are modeled over 105
596 days (top to bottom) using reported data from 4 global regions: Massachusetts, Los Angeles,
597 New York City, and São José do Rio Preto in Brazil (left to right). The COVID-19 population
598 spread and outcomes are modeled under a Rapid Testing Protocol with variable testing
599 frequencies ranging from 1-21 days between tests, and variable test performances: 90%
600 specificity with 90% sensitivity (A), 70% sensitivity (B), 50% sensitivity (C), and 30%
601 sensitivity (D); and 80% specificity with 90% sensitivity (E), 70% sensitivity (F), 50%
602 sensitivity (G), and 30% sensitivity (H). This protocol is compared to a symptom-based Rapid
603 Testing protocol and a symptom-based qRT-PCR protocol.

604

605 **Supplementary Fig. 4. Effect of Rapid Testing Protocol under variable testing sensitivities**
606 **and increasing frequency under the *SIDHRE-Q* Model.** The Cumulative Infections,
607 Maximum Simultaneously Hospitalized, and Deceased populations are modeled for
608 Massachusetts, Los Angeles, New York City, and São José do Rio Preto in Brazil. The effect of
609 increasing frequency of testing is modeled for various testing sensitivities (30%-90%) with an
610 80% specificity.

611

612

613 **Supplementary Fig. 5. Time series of the four fitted parameters α , ν , μ , and τ (left to right)**

614 **for MA, LA, NYC, and SJRP (top to bottom).** See Table 4 in the Methods section for an

615 explanation of the parameters. The values are extracted every seven days from data provided by

616 the respective regions. The parameters vary significantly over time and location. Flat points

617 occur during the seven day windows where the parameters are held constant. The fitting

618 procedure is also outlined in the Methods section.

619

620 **Supplementary Fig. 6. Time series of the three fitted pieces of data Cumulative Cases, Daily**

621 **Hospitalized, and Cumulative Deaths (left to right) for each county receiving testing in CA;**

622 Ventura (2A), Stanislaus (2B), Santa Clara (2C), San Joaquin (2D), San Francisco (2E), San

623 Diego (2F), San Bernardino (2G), Sacramento (2H), Orange (2I), Los Angeles (2J), Kern (2K),

624 Fresno (2L), Alameda (2M). The counties included satisfy two requirements: population greater

625 than 1.5% of the total CA population and nonzero total number of deaths at each point in time.

626 The fitting procedure is outlined in the Methods section.

627

628

629 **References**

630 1. Coronavirus Disease (COVID-19) Situation Reports. [https://www.who.int/emergencies/diseases/novel-](https://www.who.int/emergencies/diseases/novel-coronavirus-2019/situation-reports)
631 [coronavirus-2019/situation-reports](https://www.who.int/emergencies/diseases/novel-coronavirus-2019/situation-reports).

632 2. Menkir, T. F. *et al.* Estimating the number of undetected COVID-19 cases exported internationally from all of
633 China. *medRxiv* (2020) doi:10.1101/2020.03.23.20038331.

634 3. Ivorra, B., Ferrández, M. R., Vela-Pérez, M. & Ramos, A. M. Mathematical modeling of the spread of the
635 coronavirus disease 2019 (COVID-19) taking into account the undetected infections. The case of China.

636 *Commun Nonlinear Sci Numer Simul* 105303 (2020) doi:10.1016/j.cnsns.2020.105303.

- 637 4. Salathé, M. *et al.* COVID-19 epidemic in Switzerland: on the importance of testing, contact tracing and
638 isolation. *Swiss Med Wkly* **150**, w20225 (2020).
- 639 5. Lau, H. *et al.* Evaluating the massive underreporting and undertesting of COVID-19 cases in multiple global
640 epicenters. *Pulmonology* (2020) doi:10.1016/j.pulmoe.2020.05.015.
- 641 6. Silverman, J. D., Hupert, N. & Washburne, A. D. Using influenza surveillance networks to estimate state-
642 specific prevalence of SARS-CoV-2 in the United States. *Science Translational Medicine* (2020)
643 doi:10.1126/scitranslmed.abc1126.
- 644 7. Böhning, D., Rocchetti, I., Maruotti, A. & Holling, H. Estimating the undetected infections in the Covid-19
645 outbreak by harnessing capture-recapture methods. *Int. J. Infect. Dis.* **97**, 197–201 (2020).
- 646 8. Baek, Y. H. *et al.* Development of a reverse transcription-loop-mediated isothermal amplification as a rapid
647 early-detection method for novel SARS-CoV-2. *Emerg Microbes Infect* **9**, 998–1007 (2020).
- 648 9. Leo, L. Mylab gets commercial approval from ICMR for Covid-19 antigen rapid testing kit. *Livemint*
649 [https://www.livemint.com/news/india/mylab-gets-commercial-approval-from-icmr-for-covid-19-antigen-rapid-](https://www.livemint.com/news/india/mylab-gets-commercial-approval-from-icmr-for-covid-19-antigen-rapid-testing-kit-11595434040321.html)
650 [testing-kit-11595434040321.html](https://www.livemint.com/news/india/mylab-gets-commercial-approval-from-icmr-for-covid-19-antigen-rapid-testing-kit-11595434040321.html) (2020).
- 651 10. Dey, S. Coronavirus testing: Rapid antigen tests now make up nearly half of daily checks | India News - Times
652 of India. *The Times of India* [https://timesofindia.indiatimes.com/india/rapid-antigen-tests-now-make-up-nearly-](https://timesofindia.indiatimes.com/india/rapid-antigen-tests-now-make-up-nearly-half-of-daily-checks/articleshow/77340459.cms)
653 [half-of-daily-checks/articleshow/77340459.cms](https://timesofindia.indiatimes.com/india/rapid-antigen-tests-now-make-up-nearly-half-of-daily-checks/articleshow/77340459.cms).
- 654 11. Vogels, C. B. F. *et al.* Analytical sensitivity and efficiency comparisons of SARS-CoV-2 RT-qPCR primer-
655 probe sets. *Nat Microbiol* (2020) doi:10.1038/s41564-020-0761-6.
- 656 12. Larremore, D. B. *et al.* Test sensitivity is secondary to frequency and turnaround time for COVID-19
657 surveillance. *medRxiv* (2020) doi:10.1101/2020.06.22.20136309.
- 658 13. Shen, Z. *et al.* Superspreading SARS events, Beijing, 2003. *Emerging Infect. Dis.* **10**, 256–260 (2004).
- 659 14. Peiris, J. S. M. *et al.* Clinical progression and viral load in a community outbreak of coronavirus-associated
660 SARS pneumonia: a prospective study. *Lancet* **361**, 1767–1772 (2003).
- 661 15. He, X. *et al.* Temporal dynamics in viral shedding and transmissibility of COVID-19. *Nat. Med.* **26**, 672–675
662 (2020).
- 663 16. Bullard, J. *et al.* Predicting infectious SARS-CoV-2 from diagnostic samples. *Clin. Infect. Dis.* (2020)
664 doi:10.1093/cid/ciaa638.

- 665 17. Giordano, G. *et al.* Modelling the COVID-19 epidemic and implementation of population-wide interventions in
666 Italy. *Nat. Med.* **26**, 855–860 (2020).
- 667 18. Choi, S. & Ki, M. Estimating the reproductive number and the outbreak size of COVID-19 in Korea. *Epidemiol*
668 *Health* **42**, e2020011 (2020).
- 669 19. Wei, Y. Y. *et al.* [Fitting and forecasting the trend of COVID-19 by SEIR(+CAQ) dynamic model]. *Zhonghua*
670 *Liu Xing Bing Xue Za Zhi* **41**, 470–475 (2020).
- 671 20. Yang, Z. *et al.* Modified SEIR and AI prediction of the epidemics trend of COVID-19 in China under public
672 health interventions. *J Thorac Dis* **12**, 165–174 (2020).
- 673 21. Cao, S., Feng, P. & Shi, P. [Study on the epidemic development of COVID-19 in Hubei province by a modified
674 SEIR model]. *Zhejiang Da Xue Xue Bao Yi Xue Ban* **49**, 178–184 (2020).
- 675 22. Huang, R., Liu, M. & Ding, Y. Spatial-temporal distribution of COVID-19 in China and its prediction: A data-
676 driven modeling analysis. *J Infect Dev Ctries* **14**, 246–253 (2020).
- 677 23. Godio, A., Pace, F. & Vergnano, A. SEIR Modeling of the Italian Epidemic of SARS-CoV-2 Using
678 Computational Swarm Intelligence. *Int J Environ Res Public Health* **17**, (2020).
- 679 24. Gatto, M. *et al.* Spread and dynamics of the COVID-19 epidemic in Italy: Effects of emergency containment
680 measures. *Proc. Natl. Acad. Sci. U.S.A.* **117**, 10484–10491 (2020).
- 681 25. Hou, C. *et al.* The effectiveness of quarantine of Wuhan city against the Corona Virus Disease 2019 (COVID-
682 19): A well-mixed SEIR model analysis. *J. Med. Virol.* **92**, 841–848 (2020).
- 683 26. Zhou, T. *et al.* Preliminary prediction of the basic reproduction number of the Wuhan novel coronavirus 2019-
684 nCoV. *J Evid Based Med* **13**, 3–7 (2020).
- 685 27. Reno, C. *et al.* Forecasting COVID-19-Associated Hospitalizations under Different Levels of Social Distancing
686 in Lombardy and Emilia-Romagna, Northern Italy: Results from an Extended SEIR Compartmental Model. *J*
687 *Clin Med* **9**, (2020).
- 688 28. Yu, F. *et al.* Quantitative Detection and Viral Load Analysis of SARS-CoV-2 in Infected Patients. *Clin. Infect.*
689 *Dis.* **71**, 793–798 (2020).
- 690 29. Rao, S. N., Manissero, D., Steele, V. R. & Pareja, J. A Narrative Systematic Review of the Clinical Utility of
691 Cycle Threshold Values in the Context of COVID-19. *Infect Dis Ther* 1–14 (2020) doi:10.1007/s40121-020-
692 00324-3.

- 693 30. Alizargar, J. Risk of reactivation or reinfection of novel coronavirus (COVID-19). *J. Formos. Med. Assoc.* **119**,
694 1123 (2020).
- 695 31. Batisse, D. *et al.* Clinical recurrences of COVID-19 symptoms after recovery: viral relapse, reinfection or
696 inflammatory rebound? *J. Infect.* (2020) doi:10.1016/j.jinf.2020.06.073.
- 697 32. Deng, W. *et al.* Primary exposure to SARS-CoV-2 protects against reinfection in rhesus macaques. *Science*
698 (2020) doi:10.1126/science.abc5343.
- 699 33. Ota, M. Will we see protection or reinfection in COVID-19? *Nat. Rev. Immunol.* **20**, 351 (2020).
- 700 34. Victor Okhue, A. Estimation of the Probability of Reinfection With COVID-19 by the Susceptible-Exposed-
701 Infectious-Removed-Undetectable-Susceptible Model. *JMIR Public Health Surveill* **6**, e19097 (2020).
- 702 35. Gu, Y. COVID-19 Projections Using Machine Learning. *COVID-19 Projections Using Machine Learning*
703 <https://covid19-projections.com/>.
- 704 36. Stadlbauer, D. *et al.* Seroconversion of a city: Longitudinal monitoring of SARS-CoV-2 seroprevalence in New
705 York City. *medRxiv* 2020.06.28.20142190 (2020) doi:10.1101/2020.06.28.20142190.
- 706 37. Goodnough, A. & Shear, M. D. The U.S.'s Slow Start to Coronavirus Testing: A Timeline. *The New York*
707 *Times* (2020).
- 708 38. Shear, M. D. *et al.* The Lost Month: How a Failure to Test Blinded the U.S. to Covid-19. *The New York Times*
709 (2020).
- 710 39. Kaplan, S. & Thomas, K. Despite Promises, Testing Delays Leave Americans 'Flying Blind'. *The New York*
711 *Times* (2020).
- 712 40. de Souza, W. M. *et al.* Epidemiological and clinical characteristics of the COVID-19 epidemic in Brazil.
713 *Nature Human Behaviour* **4**, 856–865 (2020).
- 714 41. Mervosh, S. & Fernandez, M. 'It's Like Having No Testing': Coronavirus Test Results Are Still Delayed. *The*
715 *New York Times* (2020).
- 716 42. Gostic, K., Gomez, A. C., Mummah, R. O., Kucharski, A. J. & Lloyd-Smith, J. O. Estimated effectiveness of
717 symptom and risk screening to prevent the spread of COVID-19. *eLife* **9**, e55570 (2020).
- 718 43. Zitek, T. The Appropriate Use of Testing for COVID-19. *West J Emerg Med* **21**, 470–472 (2020).
- 719 44. Bosch, I. *et al.* Rapid antigen tests for dengue virus serotypes and Zika virus in patient serum. *Sci Transl Med* **9**,
720 (2017).

- 721 45. Massachusetts Department of Public Health. COVID-19 Response Reporting. *Mass.gov*
722 <https://www.mass.gov/info-details/covid-19-response-reporting>.
- 723 46. California Department of Public Health. COVID-19 Cases - California Open Data.
724 <https://data.ca.gov/dataset/covid-19-cases>.
- 725 47. California Department of Public Health. COVID-19 Hospital Data - California Open Data.
726 <https://data.ca.gov/dataset/covid-19-hospital-data>.
- 727 48. Department of Health and Human Hygiene. COVID-19 Daily Counts of Cases, Hospitalizations, and Deaths |
728 NYC Open Data. [https://data.cityofnewyork.us/Health/COVID-19-Daily-Counts-of-Cases-Hospitalizations-](https://data.cityofnewyork.us/Health/COVID-19-Daily-Counts-of-Cases-Hospitalizations-an/rc75-m7u3)
729 [an/rc75-m7u3](https://data.cityofnewyork.us/Health/COVID-19-Daily-Counts-of-Cases-Hospitalizations-an/rc75-m7u3).
- 730 49. Sao Jose do Rio Preto Public Health Office. *COVID-19 Surveillance Data, Sao Jose do Rio Preto*.
- 731 50. New York State Government. Daily Hospitalization Summary by Region. *New York Forward*
732 <https://forward.ny.gov/daily-hospitalization-summary-region>.
- 733 51. Massachusetts General Hospital Institute for Technology Assessment. COVID-19 Simulator - Methodology.
734 https://www.covid19sim.org/images/docs/COVID-19_simulator_methodology_download_20200507.pdf.
- 735 52. CDC. Coronavirus Disease 2019 (COVID-19). *Centers for Disease Control and Prevention*
736 <https://www.cdc.gov/coronavirus/2019-ncov/cases-updates/commercial-lab-surveys.html> (2020).
- 737 53. SciPy.org — SciPy.org. <https://www.scipy.org/>.
- 738 54. NumPy. <https://numpy.org/>.
- 739 55. Non-Linear Least-Squares Minimization and Curve-Fitting for Python — Non-Linear Least-Squares
740 Minimization and Curve-Fitting for Python. <https://lmfit.github.io/lmfit-py/>.
- 741 56. Matplotlib: Python plotting — Matplotlib 3.3.1 documentation. <https://matplotlib.org/>.
- 742 57. Plotly: The front-end for ML and data science models. <https://plotly.com/>.

743

744

745 **Acknowledgments**

746

General: We thank Professor Lee Gehrke for critical reading of the manuscript.

747 **Funding:** EN is funded by Tufts University DISC Seed Grant. MLN is supported by a
748 FAPESP grant (#2020/04836-0) and is a CNPq Research Fellow. AFV is supported by a
749 FAPESP Fellow grant (#18/17647-0). GRFC is supported by a FAPESP Fellow grant
750 (#20/07419-0). BHGAM is supported by a FAPESP Scholarship (#19/06572-2). The
751 funders had no role in the design of the study; in the collection, analyses, or interpretation
752 of data; in the writing of the manuscript, or in the decision to publish the results.

753 **Author contributions:** Conceptualization: BBH. Formal analysis: BN, AB, AR, MB,
754 NS, ARG, AV, GCDS, TMILDS, BHGAM, MMM, GRFC, FQ, AFNR, MLG, ENN, IB,
755 BBH. Funding acquisition: IB, BBH. Investigation: BN, AB, AR, MB, NS, ARG, AV,
756 GCDS, TMILDS, BHGAM, MMM, GRFC, FQ, AFNR, MLG, ENN, IB, BBH.

757 Methodology: BN, AB, AR, MB, NS, ARG, AV, GCDS, TMILDS, BHGAM, MMM,
758 GRFC, FQ, AFNR, MLG, ENN, IB, BBH. Project administration: MLN, IB, BBH.
759 Resources: MLN, IB, BBH. Supervision: MB, MLN, ENN, IB, BBH. Validation: BN,
760 AB, AR, MB, ENN, BBH. Visualization: BN, AB, AR, MB, AV, ENN, BBH. Writing—
761 original draft: AR, BBH. Writing—review and editing: BN, AB, AR, MB, NS, ARG,
762 AV, GCDS, TMILDS, BHGAM, MMM, GRFC, FQ, AFNR, MLG, ENN, IB, BBH.

763 **Competing interests:** BN, AB, AR, MB, NS, AG, IB, and BBH are employed by or
764 affiliated with E25Bio Inc. (www.e25bio.com), a company that develops diagnostics for
765 epidemic viruses.

766

767

768

769

770
771
772
773
774
775
776
777
778
779
780
781
782
783
784

Figures and Tables

TABLES

Table 1. Data summary of direct antigen rapid test (DART) for detection of SARS-CoV-2 nucleocapsid protein and DART for detection of SARS-CoV-2 spike glycoprotein performance in comparison to qRT-PCR results. Sensitivity, specificity, Positive predictive value, (PPV) negative predictive value (NPV), prevalence, and overall agreement are calculated for increasing PCR cycle threshold (Ct) values.

	Cycle threshold (Ct) value	Total Cases	DART Positives	DART Negatives	Sensitivity	95% Confidence Interval (semi-interval)	Specificity	95% Confidence Interval (semi-interval)	Positive Predictive Value (PPV)	Negative Predictive Value (NPV)	Prevalence	Overall Agreement
DART (nucleocapsid protein)	SARS-CoV-2 (Gene Average)											
	< 20	114	24	90	95.8%	4.6%	91.1%	2.9%	74.2%	98.8%	21.1%	92.1%
	< 25	143	53	90	90.6%	3.9%	91.1%	2.9%	85.7%	94.3%	37.1%	90.9%
	< 30	168	78	90	83.3%	4.1%	91.1%	2.9%	89.0%	86.3%	46.4%	87.5%
	< 35	189	99	90	79.8%	3.9%	91.1%	2.9%	90.8%	80.4%	52.4%	85.2%
< 40	190	100	90	80.0%	3.9%	91.1%	2.9%	90.9%	80.4%	52.6%	85.3%	
DART (spike glycoprotein)	SARS-CoV-2 (Gene Average)											
	< 10	51	2	49	100.0%	20.9%	85.7%	4.9%	22.2%	98.9%	3.9%	86.3%
	< 15	72	23	49	100.0%	2.8%	85.7%	4.9%	76.7%	98.9%	31.9%	90.3%
	< 20	90	41	49	97.6%	2.8%	85.7%	4.9%	85.1%	96.6%	45.6%	91.1%
	< 25	111	62	49	91.9%	3.4%	85.7%	4.9%	89.1%	89.4%	55.9%	89.2%
< 30	121	72	49	84.7%	4.1%	85.7%	4.9%	89.7%	79.2%	59.5%	85.1%	
< 35	121	72	49	84.7%	4.1%	85.7%	4.9%	89.7%	79.2%	59.5%	85.1%	

786

787

788

789

790 **Table 2. Clinical validation summary for the direct antigen rapid test (DART) for SARS-**

791 **CoV-2 nucleocapsid protein evaluated using 190 retrospectively collected patient nasal**

792 **swab specimens.**

793

All Data Summary								
		qRT-PCR (gene average)					95% Confidence Interval	
		+	-	Total	Sensitivity	80.0%	76.1%	83.9%
DART (nucleocapsid protein)	+	80	8	88	Specificity	91.1%	88.2%	94.0%
	-	20	82	102	Positive Predictive Value	90.9%	87.9%	93.9%
Total		100	90	190	Negative Predictive Value	80.4%	76.6%	84.2%
					Prevalence	52.6%	47.8%	57.5%
					Overall Agreement	85.3%	82.8%	87.8%

794

795

796

797

798

799

800

801

802 **Table 3. Clinical validation summary for the SARS-CoV-2 direct antigen rapid test**
 803 **(DART) for SARS-SoC-2 spike glycoprotein evaluated using 121 retrospectively collected**
 804 **patient nasopharyngeal swab specimens.**

805

806

All Data Summary								
		qRT-PCR (gene average)					95% Confidence Interval	
		+	-	Total	Sensitivity	84.7%	80.6%	88.9%
DART (spike glycoprotein)	+	61	7	68	Specificity	85.7%	80.8%	90.6%
	-	11	42	53	Positive Predictive Value	89.7%	86.2%	93.2%
Total		72	49	121	Negative Predictive Value	79.2%	73.6%	84.9%
					Prevalence	59.5%	53.9%	65.1%
					Overall Agreement	85.1%	82.0%	88.3%

807

808

809

810

811

812

813

814

815

816

817

818 **Table 4. Details of parameter values used for *SIDHRE-Q* Model.**

819

Parameter	Details & Statistics			
α	α is the probability that an interaction between an undetected infected person and an uninfected person results in a new infection, divided by the average number of uninfected people an undetected infected person comes into contact with on a given day. α is estimated from the data.		Mean	St. Dev.
		MA	0.088	0.051
		LA	0.090	0.034
		NYC	0.067	0.042
		SJRP	0.121	0.042
η	η is the probability that an interaction between an infected person and an uninfected person results in a new infection, divided by the average number of uninfected people a detected infected person comes into contact with on a given day. $\eta = 0.01 \cdot \alpha$ The constant relating η, α accounts for a small but nonzero transmission due to the quarantined (detected) infected population. This value was chosen to be small, assuming a quarantined individual will only infect others with low probability.			
ν	ν is the probability that a symptomatic undetected individual is diagnosed on a given day. ν is estimated from the data. ν is multiplied by sensitivity (assume benchmark sensitivity 100% for PCR, as used when fitting).		Mean	St. Dev.
		MA	0.006	0.005
		LA	0.011	0.006
		NYC	0.0056	0.002
		SJRP	0.015	0.007
ϵ	ϵ is the probability that an asymptomatic undetected infected individual is diagnosed on a given day. $\epsilon = 0$ while fitting (during PCR symptomatic testing). $\epsilon = (\text{sensitivity}/\text{days between tests})$ when the rapid testing strategy is activated.			
λ	λ is the probability that an undetected infected individual transitions to the recovered state on a given day. $\lambda = 1/14$, or the inverse of average recovery time ⁵¹ .			
μ	μ is the probability that an infected individual develops severe symptoms on a given day and transitions into the hospitalized state. The flow from D to H is assumed to be independent of the ratio I/D , but comes only from the detected infected population, hence why it is multiplied by $(I + D)/D$. μ is estimated from the data.		Mean	St. Dev.
		MA	0.0013	9.5e-4
		LA	0.0016	2.4e-4
		NYC	0.0011	6.6e-4
		SJRP	0.0018	8.0e-4

ρ	<p>ρ is the probability that a detected infected individual transitions to the recovered state on a given day.</p> <p>$\rho = 1/14$, or the inverse of the average recovery time ⁵¹.</p>			
σ	<p>σ is the probability that a hospitalized individual transitions to the recovered state on a given day. $\sigma = 1/11$, or the inverse of the average recovery time for a hospitalized individual ⁵¹.</p>			
τ	<p>τ is the probability that a hospitalized individual expires on a given day. τ is estimated from the data.</p>		Mean	St. Dev.
		MA	0.034	0.012
		LA	0.016	0.004
		NYC	0.036	0.034
		SJRP	0.032	0.045
γ	<p>γ is the probability of entering either of the quarantine states on a given day from either the Susceptible or Recovered populations. $\gamma = 0$ while fitting (during PCR symptomatic testing). $\gamma = (1 - \text{specificity}) \times (1/\text{days between tests})$ when the rapid testing strategy is activated.</p>			
ψ	<p>ψ is the probability that an individual exits quarantine on a given day. $\psi = 1/14$, or the inverse of the quarantine period for fixed length quarantine.</p>			
Parameter	Details & Statistics			
$\bar{\alpha}$	<p>$\bar{\alpha}$ is the probability that an interaction between an undetected infected person and an uninfected person results in a new infection, divided by the average number of uninfected people an undetected infected person comes into contact with on a given day. $\bar{\alpha}$ is estimated from the data.</p>		Mean	St. Dev.
		MA	0.088	0.051
		LA	0.090	0.034
		NYC	0.067	0.042
		SJRP	0.121	0.042
$\bar{\eta}$	<p>$\bar{\eta}$ is the probability that an interaction between an infected person and an uninfected person results in a new infection, divided by the average number of uninfected people a detected infected person comes into contact with on a given day. $\bar{\eta} = 0.01 \cdot \bar{\alpha}$</p> <p>The constant relating $\bar{\eta}$, $\bar{\alpha}$ accounts for a small but nonzero transmission due to the quarantined (detected) infected population. This value was chosen to be small, assuming a quarantined individual will only infect others with low probability.</p>			
$\bar{\nu}$	<p>$\bar{\nu}$ is the probability that a symptomatic undetected individual is diagnosed on a given day. $\bar{\nu}$ is estimated from the data. $\bar{\nu}$ is multiplied by sensitivity (assume benchmark sensitivity 100% for PCR, as used when fitting).</p>		Mean	St. Dev.
		MA	0.006	0.005
		LA	0.011	0.006
		NYC	0.0056	0.002

		SJRP	0.015	0.007
$\bar{\epsilon}$	$\bar{\epsilon}$ is the probability that an asymptomatic undetected infected individual is diagnosed on a given day. $\bar{\epsilon} = 0$ while fitting (during PCR symptomatic testing). $\bar{\epsilon} = (\text{sensitivity}/\text{days between tests})$ when the rapid testing strategy is activated.			
$\bar{\lambda}$	$\bar{\lambda}$ is the probability that an undetected infected individual transitions to the recovered state on a given day. $\bar{\lambda} = 1/14$, or the inverse of average recovery time ⁵¹ .			
$\bar{\mu}$	$\bar{\mu}$ is the probability that an infected individual develops severe symptoms on a given day and transitions into the hospitalized state. The flow from \bar{D} to \bar{H} is assumed to be independent of the ratio \bar{I}/\bar{D} , but comes only from the detected infected population, hence why it is multiplied by $(\bar{I} + \bar{D})/\bar{D}$. $\bar{\mu}$ is estimated from the data.		Mean	St. Dev.
		MA	0.0013	9.5e-4
		LA	0.0016	2.4e-4
		NYC	0.0011	6.6e-4
		SJRP	0.0018	8.0e-4
$\bar{\rho}$	$\bar{\rho}$ is the probability that a detected infected individual transitions to the recovered state on a given day. $\bar{\rho} = 1/14$, or the inverse of the average recovery time ⁵¹ .			
$\bar{\sigma}$	$\bar{\sigma}$ is the probability that a hospitalized individual transitions to the recovered state on a given day. $\bar{\sigma} = 1/11$, or the inverse of the average recovery time for a hospitalized individual ⁵¹ .			
$\bar{\tau}$	$\bar{\tau}$ is the probability that a hospitalized individual expires on a given day. $\bar{\tau}$ is estimated from the data.		Mean	St. Dev.
		MA	0.034	0.012
		LA	0.016	0.004
		NYC	0.036	0.034
		SJRP	0.032	0.045
$\bar{\nu}$	$\bar{\nu}$ is the probability of entering either of the quarantine states on a given day from either the Susceptible or Recovered populations. $\bar{\nu} = 0$ while fitting (during PCR symptomatic testing). $\bar{\nu} = (1 - \text{specificity}) \times (1/\text{days between tests})$ when the rapid testing strategy is activated.			
$\bar{\psi}$	$\bar{\psi}$ is the probability that an individual exits quarantine on a given day. $\bar{\psi} = 1/14$, or the inverse of the quarantine period for fixed length quarantine.			

820

821

822

823

824 **FIGURES**

825

826 **Fig. 1. Graphical scheme displaying the relationships between the stages of quarantine and**

827 **infection in *SIDHRE-Q* model. Q-U, quarantine uninfected; S, susceptible (uninfected); I,**

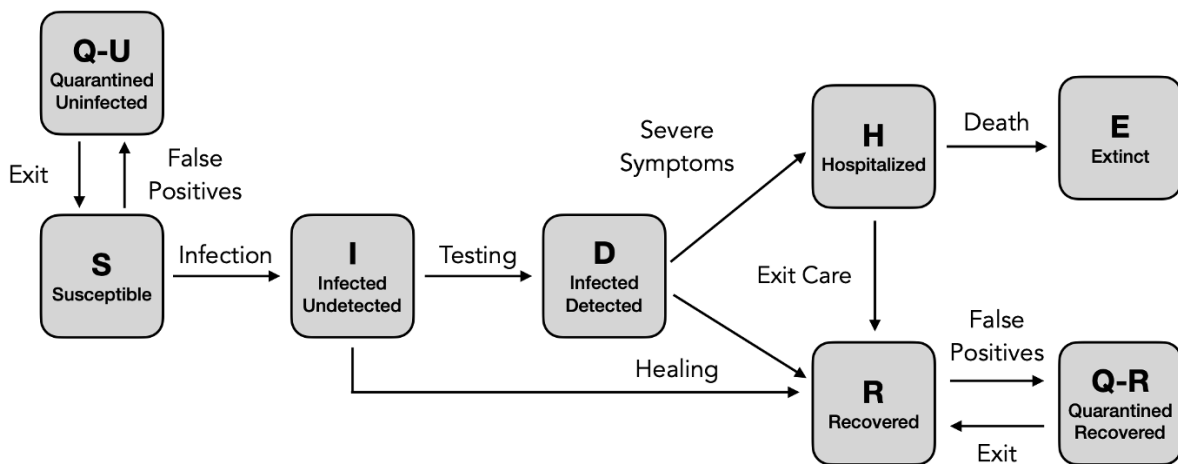
828 **infected undetected (pre-testing and infected); D, infected detected (infection diagnosis through**

829 **testing); H, hospitalized (infected with life threatening symptom progression); R, recovered**

830 **(healed); E, extinct (dead); and Q-R, quarantine recovered (healed but in quarantine by false**

831 **positive testing).**

832



833

834

835

836

837

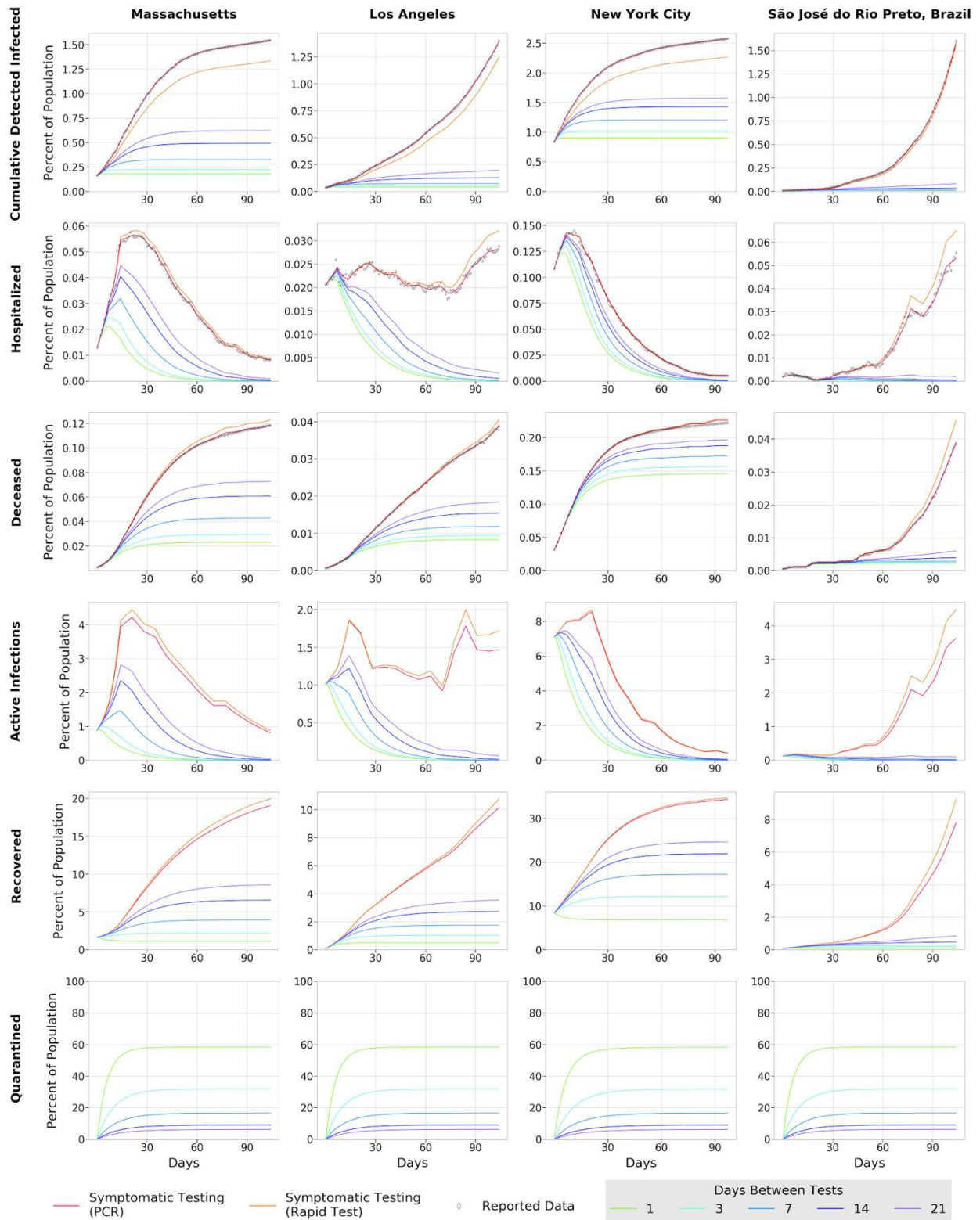
838

839

840

841

842 **Fig. 2. COVID-19 Outcomes in 3 US Regions and Brazil as a result of Frequent Rapid**
843 **Testing Protocol using the *SIDHRE-Q* Model.** The Cumulative Detected Infected,
844 Hospitalized, Deceased, Active Infections, Recovered, and Quarantined are modeled over 105
845 days (top to bottom) using reported data from 4 global regions: Massachusetts, Los Angeles,
846 New York City, and São José do Rio Preto in Brazil (left to right). The COVID-19 population
847 spread and outcomes are modeled under a Rapid Testing Protocol (sensitivity 80%, specificity
848 90%) with variable testing frequencies ranging from 1-21 days between tests. This protocol is
849 compared to a symptom-based Rapid Testing protocol and a symptom-based PCR protocol.

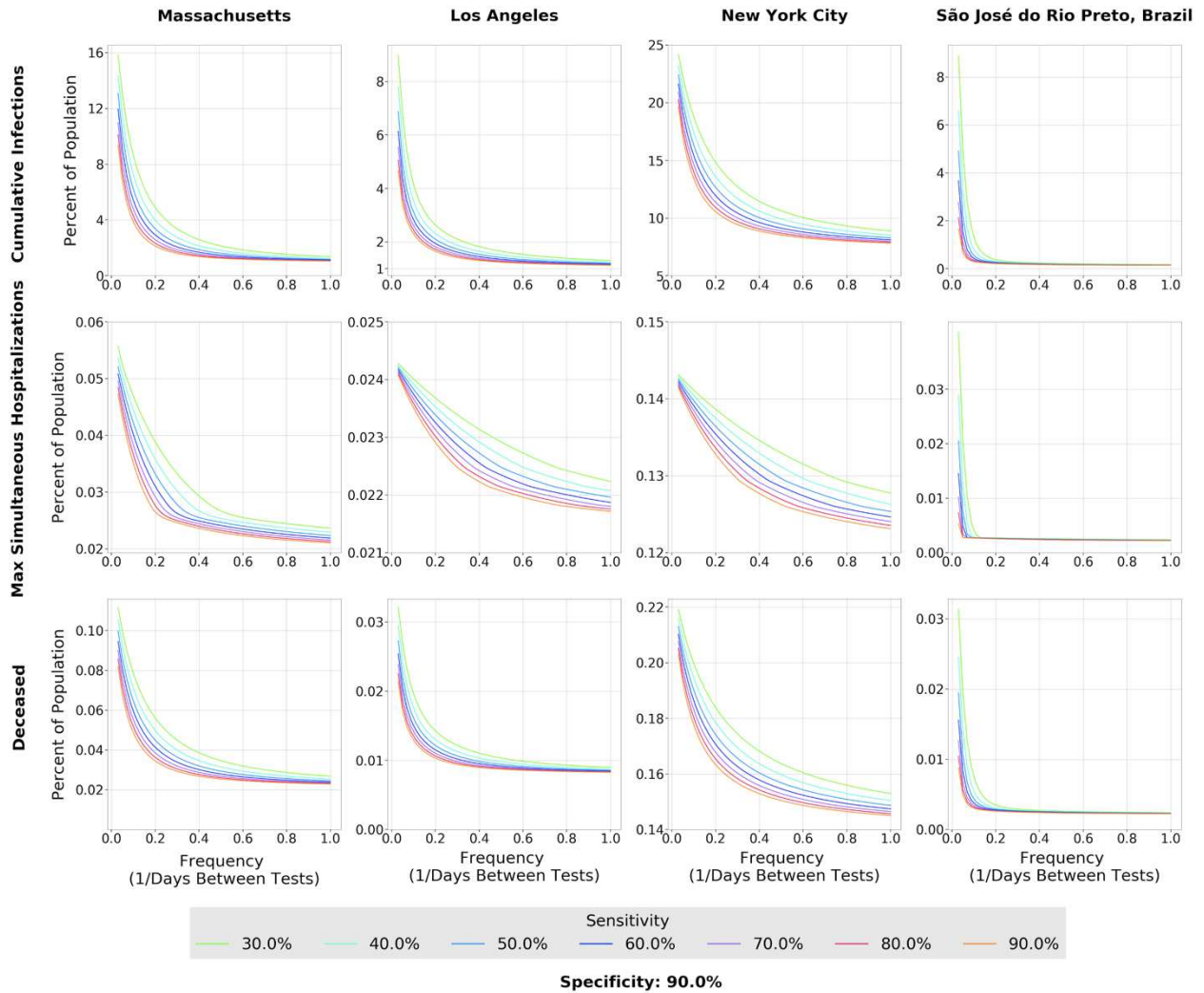


— Symptomatic Testing (PCR)
— Symptomatic Testing (Rapid Test)
◇ Reported Data
Days Between Tests
— 1
— 3
— 7
— 14
— 21

Sensitivity: 80.0% Specificity: 90.0%

850
851
852

853 **Fig. 3. Effect of Rapid Testing Protocol under variable testing sensitivities (30%-90%) and**
 854 **increasing frequency under the *SIDHRE-Q* Model.** The Cumulative Infections, Maximum
 855 Simultaneously Hospitalized, and Deceased populations are modeled for Massachusetts, Los
 856 Angeles, New York City, and São José do Rio Preto in Brazil with a 90% test specificity.



857

858

859

860

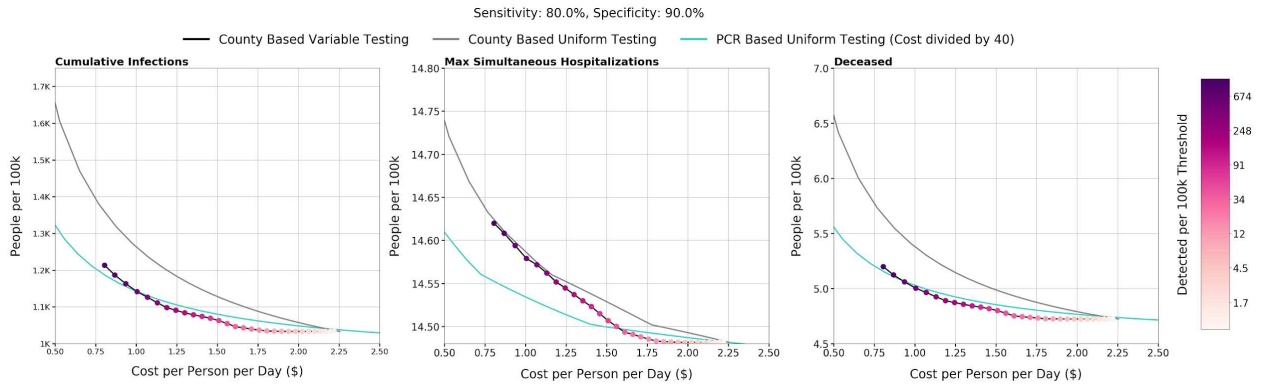
861

862

863
864
865
866
867
868
869
870
871
872
873
874
875
876
877
878
879
880
881
882
883
884
885

Fig. 4. Effect of County Based Rapid Testing strategy on COVID-19 outcomes in California. This protocol varies testing frequency in accordance to the number of recorded cases; the threshold for number of active infections which, if reached, signals to commence everyday testing (the highest frequency considered). A Rapid Test with an 80% sensitivity and 90% sensitivity versus is used in this deployment strategy. Shown is the total cost per person per day versus the cumulative infections, maximum simultaneously hospitalized, and cumulative deaths with varied thresholds for all of CA is shown. The County Based Rapid Testing strategy is compared to uniform testing, which distributes the same number of total tests used in the county strategy, albeit evenly across each county. The effects of uniform testing are modeled for both a Rapid Testing protocol and a qRT-PCR protocol (A). The effects of County Based Rapid Test Protocol and Uniform PCR Protocol on active infected detected population over time in CA are shown (B). The legend denotes the thresholds at which testing frequency is determined, the testing frequencies, the percent of CA population under the strategy, and the cost per person per day.

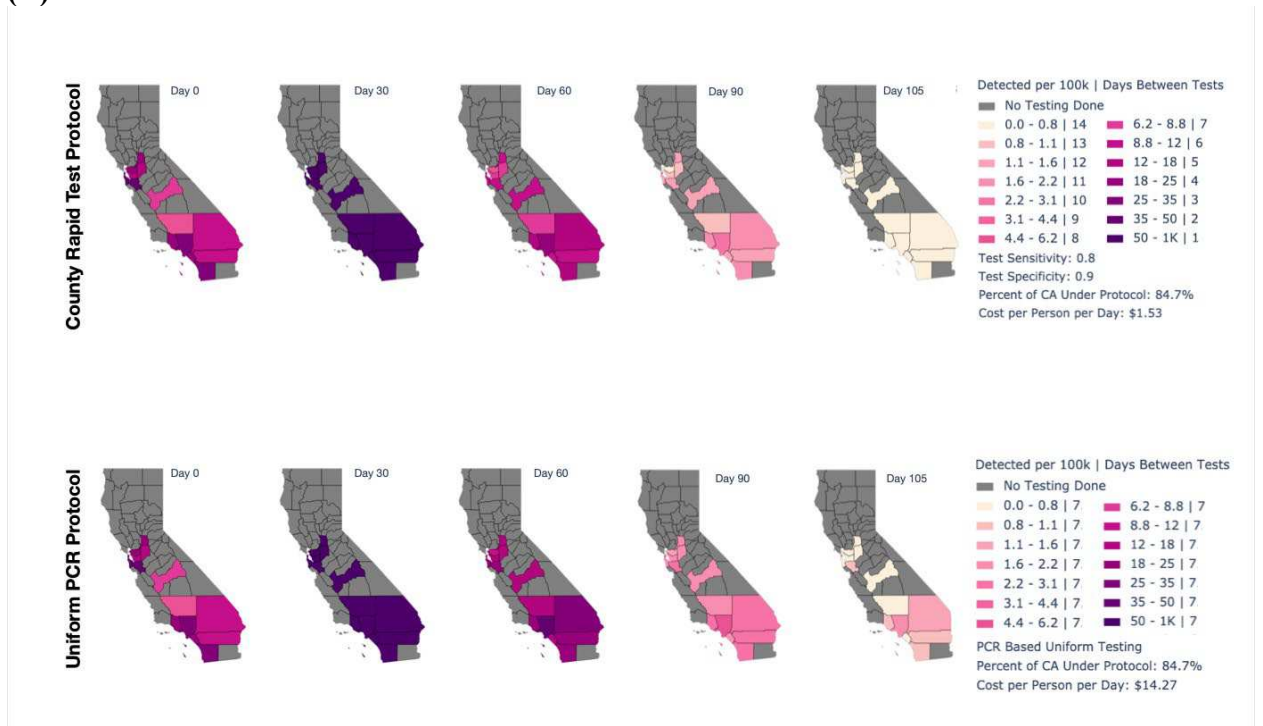
(A)



886

887

888 (B)



889

Figures

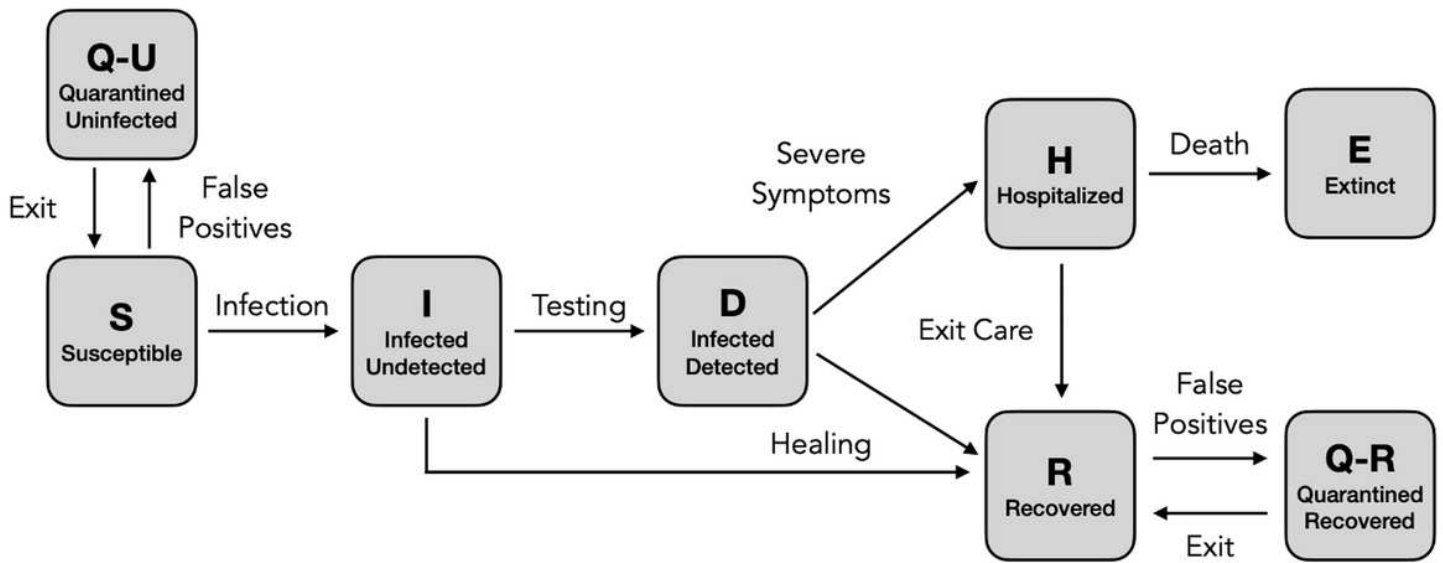


Figure 1

Graphical scheme displaying the relationships between the stages of quarantine and infection in SIDHRE-Q model. Q-U, quarantine uninfected; S, susceptible (uninfected); I, infected undetected (pre-testing and infected); D, infected detected (infection diagnosis through testing); H, hospitalized (infected with life threatening symptom progression); R, recovered (healed); E, extinct (dead); and Q-R, quarantine recovered (healed but in quarantine by false positive testing).

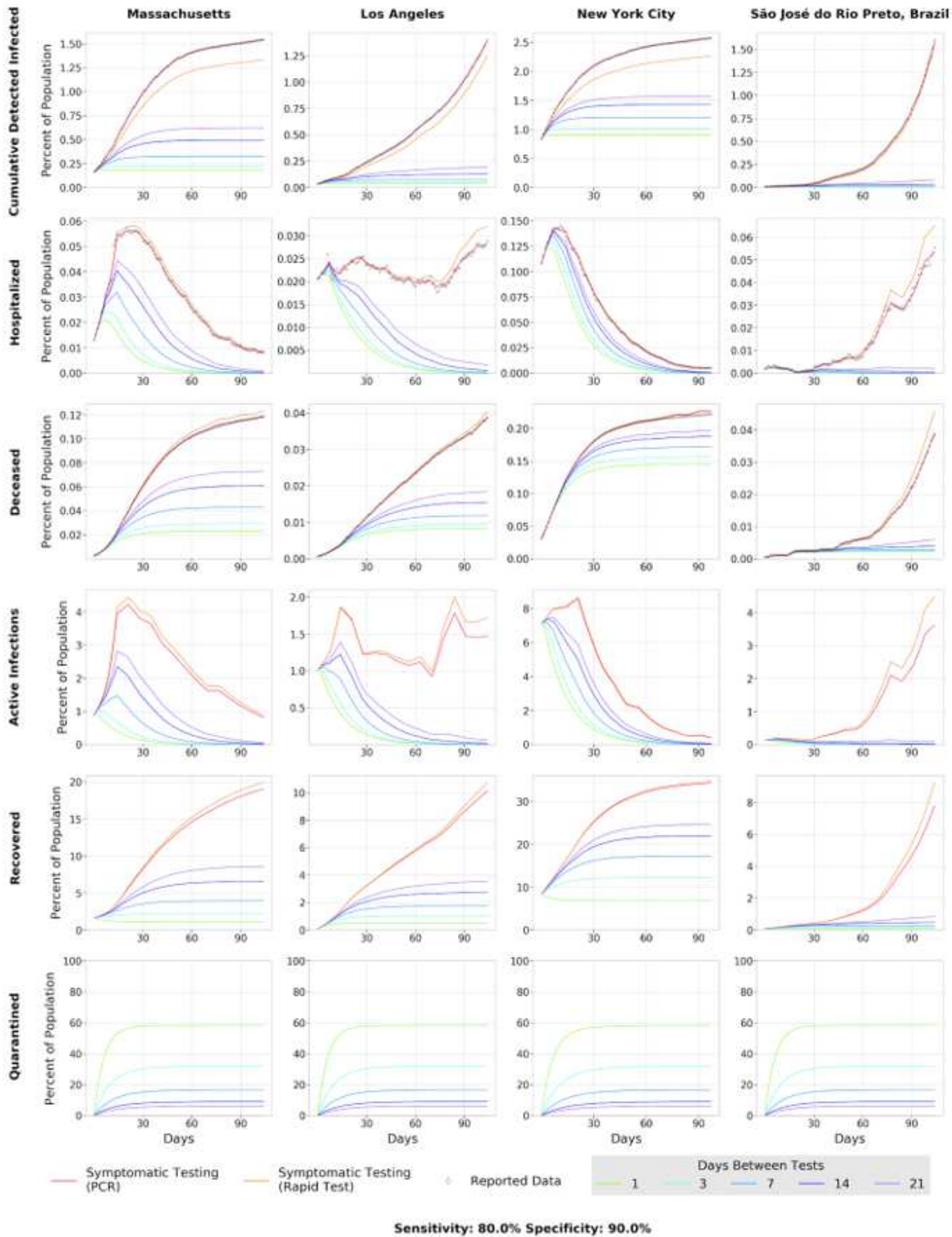


Figure 2

COVID-19 Outcomes in 3 US Regions and Brazil as a result of Frequent Rapid Testing Protocol using the SIDHRE-Q Model. The Cumulative Detected Infected, Hospitalized, Deceased, Active Infections, Recovered, and Quarantined are modeled over 105 days (top to bottom) using reported data from 4 global regions: Massachusetts, Los Angeles, New York City, and São José do Rio Preto in Brazil (left to right). The COVID-19 population spread and outcomes are modeled under a Rapid Testing Protocol (sensitivity 80%,

specificity 90%) with variable testing frequencies ranging from 1-21 days between tests. This protocol is compared to a symptom-based Rapid Testing protocol and a symptom-based PCR protocol.

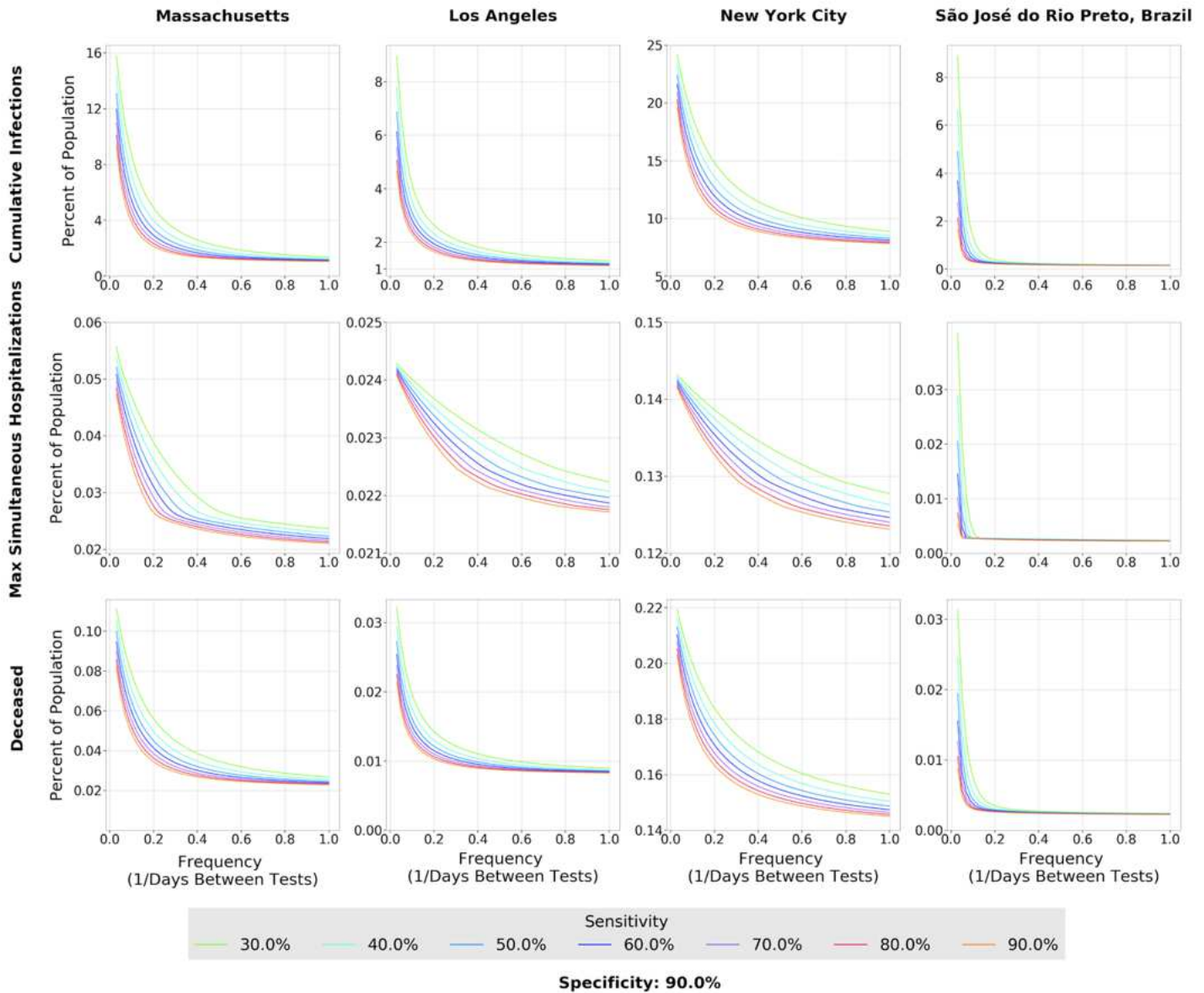


Figure 3

Effect of Rapid Testing Protocol under variable testing sensitivities (30%-90%) and increasing frequency under the SIDHRE-Q Model. The Cumulative Infections, Maximum Simultaneously Hospitalized, and Deceased populations are modeled for Massachusetts, Los Angeles, New York City, and São José do Rio Preto in Brazil with a 90% test specificity.

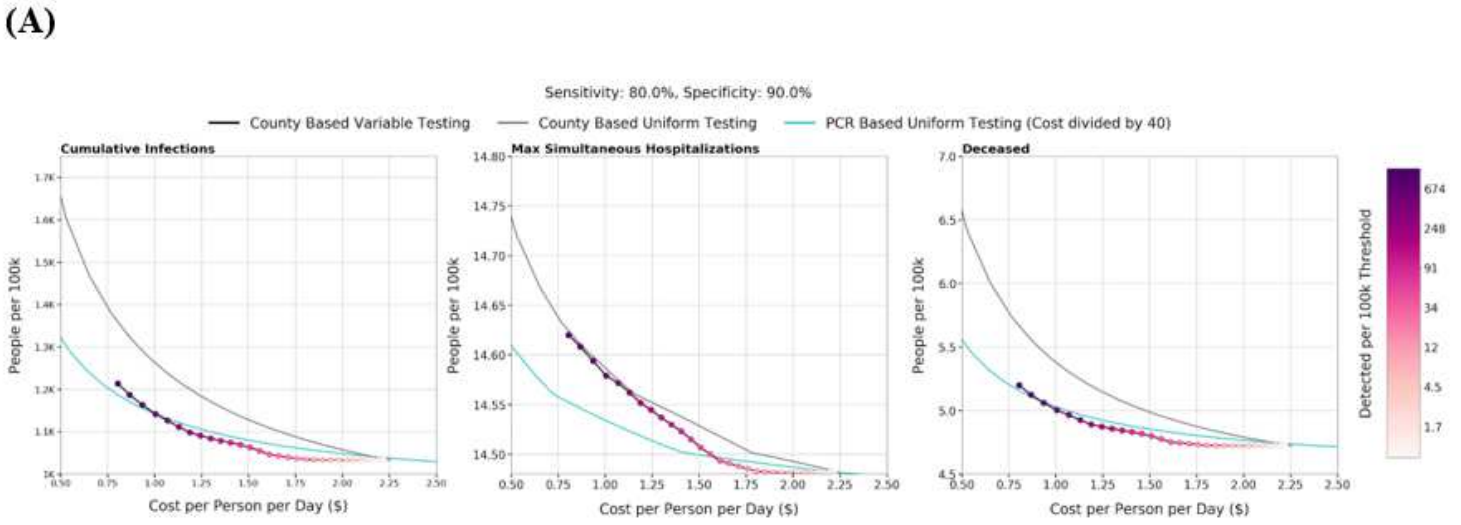


Figure 4

Effect of County Based Rapid Testing strategy on COVID-19 outcomes in California. This protocol varies testing frequency in accordance to the number of recorded cases; the threshold for number of active infections which, if reached, signals to commence everyday testing (the highest frequency considered). A Rapid Test with an 80% sensitivity and 90% sensitivity versus is used in this deployment strategy. Shown is the total cost per person per day versus the cumulative infections, maximum simultaneously

hospitalized, and cumulative deaths with varied thresholds for all of CA is shown. The County Based Rapid Testing strategy is compared to uniform testing, which distributes the same number of total tests used in the county strategy, albeit evenly across each county. The effects of uniform testing are modeled for both a Rapid Testing protocol and a qRT-PCR protocol (A). The effects of County Based Rapid Test Protocol and Uniform PCR Protocol on active infected detected population over time in CA are shown (B). The legend denotes the thresholds at which testing frequency is determined, the testing frequencies, the percent of CA population under the strategy, and the cost per person per day.

Supplementary Files

This is a list of supplementary files associated with this preprint. Click to download.

- [11062020NatureCommSupplementaryMaterial.docx](#)